AIMS Mathematics, 10(7): 16157–16199.
DOI: 10.3934/math.2025724
Received: 19 March 2025
Revised: 30 June 2025
Accepted: 07 July 2025
Published: 17 July 2025

https://www.aimspress.com/journal/Math

Research article

Dynamic analysis and optimal control of a fractional-order epidemic model with nucleic acid detection and individual protective awareness: A Malaysian case study

Rui Hu[1], **Elayaraja Aruchunan**[2,*], **Muhamad Hifzhudin Noor Aziz**[1], **Cheng Cheng**[1] **and Benchawan Wiwatanapataphee**[3]

[1] Institute of Mathematical Sciences, Universiti Malaya 50603, Kuala Lumpur, Malaysia

[2] Department of Decision Science, Universiti Malaya 50603, Kuala Lumpur, Malaysia

[3] School of Elec Eng, Comp and Math Sci (EECMS), Faculty of Science and Engineering, Curtin University, Kent Street, Bently, Perth 6102 WA, Australia

* **Correspondence:** Email: elayarajah@um.edu.my.

Abstract: In this paper, we present a Caputo fractional-order COVID-19 model that incorporates nucleic acid testing and individual protective awareness to capture memory effects and the interaction of non-pharmaceutical interventions. We proved the existence, non-negativity, and boundedness of solutions and derived the basic reproduction number R_0 using the next-generation matrix method. Stability analysis showed that the disease-free equilibrium is globally asymptotically stable when $R_0 < 1$, and the endemic equilibrium is globally asymptotically stable when $R_0 > 1$. Numerical simulations using the PECE scheme of the Adams–Bashforth–Moulton method validate the theoretical results and demonstrate the role of the fractional-order parameter α in capturing transmission memory. Model parameters were estimated using a hybrid genetic algorithm-least squares approach calibrated with Malaysian COVID-19 data. The proposed model outperformed both integer-order and simplified fractional SEIR models in replicating real-world dynamics. Sensitivity and uncertainty analyses identified protective awareness and testing intensity as key factors in mitigating epidemic severity. We also formulated an optimal control problem, applying Pontryagin's maximum principle to derive six intervention strategies. Cost-effectiveness analysis showed that combined interventions are superior to single strategies, proving effective and economically viable under Malaysia's healthcare constraints.

Keywords: COVID-19; fractional order; Caputo operator; non-pharmacological interventions; optimal control; cost-efficacy analysis
Mathematics Subject Classification: 26A33, 34A08, 92D30, 49N99

1. Introduction

COVID-19 emerged in late 2019 and, owing to its remarkable transmissibility, quickly overwhelmed health systems, economies, and daily life worldwide. During the initial phase, hospitals faced severe shortages of beds, staff, and personal protective equipment. To interrupt transmission, many countries enacted lockdowns and mandatory home isolation, precipitating economic stagnation, rising unemployment, and social unrest [1–3]. In Malaysia, authorities swiftly designated dedicated treatment centers, expanded laboratory testing capacity, and enforced stringent movement controls to curb community spread. Nonetheless, the nation incurred substantial economic losses that reverberated from household incomes to international trade [4].

Mathematical models are essential for understanding COVID-19 transmission and evaluating interventions. Classical compartmental frameworks, initially suggested by Kermack and McKendrick in 1927 [5], most notably the Susceptible–Infectious–Recovered (SIR) model, partition the population into discrete epidemiological states and describe the flow between these states via systems of integer-order ordinary differential equations. Researchers have further extended these frameworks by adding new compartments or mechanisms to reflect real world complexity and have applied them extensively to COVID-19. These formulations yield analytical expressions for key metrics such as the basic reproduction number R_0, the timing and magnitude of peak incidence, and the final outbreak size, thus providing fundamental insights into threshold effects and early public health decision making [6–9]. Building on these models, researchers have gradually introduced more realistic assumptions and complex interactions, thereby enhancing the models' ability to forecast epidemic trends and evaluate intervention strategies [10–13].

Moreover, fractional order models, which use a power law kernel to incorporate memory and hereditary effects, have rapidly emerged in epidemiology, accurately capturing the lasting influence of past disease states on current transmission dynamics. These models have achieved significant success in COVID-19 research [14–17] and have been widely applied to dynamical systems studies [18–21]. To advance practical implementation, researchers have also developed analytical frameworks and efficient numerical algorithms covering stability analysis, parameter estimation, and simulation based forecasting, thereby highlighting the broad applicability and versatility of fractional order modeling [22–24]. Among these works, Denu and Kermasaour used a fractional-order COVID-19 model with lockdown to evaluate how movement restrictions affect transmission [25]. Aba Oud et al. incorporated quarantine, isolation, and environmental viral load, highlighting fractional modeling's accuracy in capturing memory effects [26]. Paul et al. focused on a fractional-order Susceptible-Exposed-Infectious-Quarantined-Recovered-Deceased (SEIQRD) model in Italy, showing how such modeling and public health measures can slow outbreaks [27].

Fractional calculus offers multiple definitions of fractional derivatives, including the Caputo, Riemann-Liouville, Grünwald-Letnikov, Hadamard, and Riesz operators, which differ markedly in their theoretical formulations and numerical demands [28, 29]. The Riemann Liouville derivative requires fractional-order initial conditions that often lack clear physical interpretation, complicating model setup and parameter fitting, while the Grünwald-Letnikov derivative demands extensive memory storage and converges slowly, leading to high computational cost and inefficiency; and the Hadamard and Riesz operators are tailored to spatial-fractional processes and thus have limited relevance for time-fractional compartmental models. In contrast, the Caputo derivative aligns naturally with classical

ordinary differential equation frameworks by accepting integer-order initial conditions, captures memory effects through a power-law convolution kernel, and can be discretized efficiently and accurately using mature schemes such as the Adams-Bashforth-Moulton predictor-corrector method to ensure robust long-term simulation performance [30, 31].

In the early stage of the COVID-19 pandemic, when vaccines and effective antiviral treatments were not available, non-pharmaceutical interventions (NPIs) played a critical role in curbing the spread of the virus. Enhancing personal protective awareness and implementing large-scale nucleic acid testing have been shown to significantly reduce transmission rates, enable early case detection, and alleviate the burden on healthcare systems through timely isolation and treatment [32–34]. Building on these successful NPIs, integrating optimal control theory into epidemic models not only leverages their benefits but also optimizes the level of intervention to maximize the prevention of disease spread while reducing associated costs, thus providing more targeted strategies for resource-limited policymakers. Building on this, Baba and Bilgehan formulated a Caputo fractional-order COVID-19 transmission model and cast it as an optimal control problem by introducing two time-dependent interventions, public awareness campaigns, and quarantine/treatment measures, and demonstrated via Runge–Kutta-4 simulations that these controls significantly reduce both the infection peak and cumulative cases [35]. Trisilowati et al. proposed a Caputo fractional-order COVID-19 model with quarantine and a standard incidence rate, and, by fitting it to Indonesian COVID-19 data, showed that the fractional-order model outperforms its integer-order counterpart in calibration accuracy and 20-day forecasting [36]. In the literature, nucleic acid testing and individual protective awareness are often studied in isolation, overlooking their interactions and cumulative memory effects throughout the course of an epidemic; likewise, the absence of dynamic cost-benefit analyses for combined interventions hampers decision-makers' ability to balance testing intensity and protective adherence under resource constraints. Hence, there is an urgent need to incorporate both testing and protective awareness into a unified, memory-dependent dynamic model to comprehensively quantify their synergistic impact and economic efficiency, thereby offering more precise guidance for intervention strategy design.

To fill this gap, we take Malaysia as a case study and construct a Caputo fractional derivative-based COVID-19 model that captures the virus's inherent transmission dynamics and elucidates the roles of nucleic acid testing and individual protective awareness in epidemic control. This study not only provides decision-makers with guidance for real-time adjustment of testing intensity and awareness campaigns and supports multi-scenario simulation and evaluation, but also holds promise for application to other regions or future public health emergencies. The major contributions of this paper are as follows:

1. We formulate a fractional-order COVID-19 model incorporating nucleic acid testing and individual protective awareness, prove the existence, non-negativity, and boundedness of the model solutions, and derive the basic reproduction number R_0 using the next-generation matrix method. Furthermore, we conduct a comprehensive stability analysis of the disease-free equilibrium (DFE) and the endemic equilibrium (EE).
2. We perform numerical simulations using the predictor-evaluate-correct-evaluate (PECE) scheme of the Adams-Bashforth-Moulton (ABM) method, which not only validates the theoretical results but also reveals the memory effect of the fractional order α.
3. We employ a hybrid genetic algorithm (GA) and least squares (LSQ) to estimate and calibrate model parameters using real COVID-19 data from Malaysia, perform

error analysis, and compare the results with integer-order and simple fractional-order Susceptible–Exposed–Infectious–Recovered (SEIR) models. We also conduct sensitivity and uncertainty analyses on the parameters related to individual protective awareness and testing.

4. Based on the model, we formulate an optimal control problem, apply the Pontryagin's maximum principle (PMP) to obtain the optimal intervention strategy, and introduce cost-effectiveness indicators to compare the effects and cost-efficiency of single versus combined interventions, thus revealing how to achieve optimal epidemic control under limited resources.

The organization of this paper is as follows. In Section 2, we introduce the model formulation and the fundamental assumptions. In Section 3, we present the theoretical analysis, derive the basic reproduction number, and discuss the stability of the equilibrium points. In Section 4, we provide the numerical simulation results and discusse the impact of key parameters on epidemic transmission. In Section 5, we calibrate the model based on actual data. In Section 6, we propose the solution of the optimal control problem and conduct a cost-effectiveness analysis. Finally, in Section 7, we conclude the paper and discuss future research directions.

2. Model formulation

In this section, we develop a Caputo fractional-order COVID-19 epidemic model incorporating nucleic acid testing and individual protective awareness. The total population (N) in this model is categorized into seven compartments, including susceptible individuals (S), susceptible individuals with self-protective awareness (S_q), exposed individuals (E), individuals from the E compartment who test positive via nucleic acid testing (Q_1), infected individuals (I), individuals from the I compartment who test positive via nucleic acid testing (Q_2), and recovered individuals (R). During the model construction process, we consider the following assumptions.

- **H1**: All individuals are assumed to mix uniformly, with no clustering or network structure effects.
- **H2**: In light of evidence that COVID-19 is transmissible during the late incubation period, we have retained the infectivity of the E compartment in our model to more accurately reflect early transmission dynamics.
- **H3**: Once susceptible individuals develop protective awareness, they actively relocate to virus-free areas, thereby temporarily avoiding further infection; however, this awareness decays over time and eventually dissipates, causing them to revert to the standard susceptible state.
- **H4**: Individuals testing positive are assumed to enter quarantine immediately and cease further transmission, with no isolation failures or delays.
- **H5**: Since our model focuses on the short-term impact of nucleic acid testing and individual protective awareness on the epidemic in Malaysia, we treat all parameters as constants, neglecting dynamic effects from public health policy changes, behavioral shifts, or viral mutations.

These assumptions render the model amenable to dynamical analysis and model fitting under stable interventions and contact patterns during a short-term, single-wave outbreak, enabling precise assessment of the immediate effects of testing and protective behaviors. The framework is particularly suited to settings like Malaysia, where robust health systems, high testing rates, rapid isolation, and relatively homogeneous social networks prevail. Based on these assumptions, we extend the

conventional model using a fractional-order approach incorporating the Caputo derivative. The variables and parameters listed in Table 1 are used to formulate the model.

Table 1. Descriptions of compartments and model parameters.

Compartments	**Description**	
$S(t)$	Susceptible	
$S_q(t)$	Susceptible (self-protection)	
$E(t)$	Exposed	
$I(t)$	Infectious	
$Q_1(t)$	Quarantine (Exposed)	
$Q_2(t)$	Quarantine (Infected)	
$R(t)$	Recovered	
Parameters	**Description**	**Unit**
Λ	Population recruitment	individuals/day
ω_1	Rate at which susceptible individuals adopt protective measures	day^{-1}
ω_2	Rate at which individuals lose protective measures	day^{-1}
β_1	Effective incidence between S and E	day^{-1}
β_2	Effective incidence between S and I	day^{-1}
ϵ_1	Inverse incubation period (E)	day^{-1}
ϵ_2	Inverse incubation period (Q_1)	day^{-1}
σ_1	Proportion of positive tests (E)	dimensionless
σ_2	Proportion of positive tests (I)	dimensionless
ξ_1	Disease-induced mortality rate (I)	day^{-1}
ξ_2	Disease-induced mortality rate (Q_2)	day^{-1}
δ_1	Recovery rate (Q_1)	day^{-1}
δ_2	Recovery rate (I)	day^{-1}
δ_3	Recovery rate (Q_2)	day^{-1}
d	Natural death rate	day^{-1}

Introducing fractional-order dynamics leads to a mismatch in the differential orders across the system, which is addressed by parameter adjustments, resulting in the following model formulation.

$$\begin{cases} {}^{C}D^{\alpha}S &= \Lambda^{\alpha} + \omega_2^{\alpha} S_q - \beta_1^{\alpha} S E - \beta_2^{\alpha} S I - (\omega_1^{\alpha} + d^{\alpha}) S, \\ {}^{C}D^{\alpha}S_q &= \omega_1^{\alpha} S - (\omega_2^{\alpha} + d^{\alpha}) S_q, \\ {}^{C}D^{\alpha}E &= \beta_1^{\alpha} S E + \beta_2^{\alpha} S I - (\epsilon_1^{\alpha} + \sigma_1^{\alpha} + d^{\alpha}) E, \\ {}^{C}D^{\alpha}Q_1 &= \sigma_1^{\alpha} E - (\epsilon_2^{\alpha} + \delta_1^{\alpha} + d^{\alpha}) Q_1, \\ {}^{C}D^{\alpha}I &= \epsilon_1^{\alpha} E - (\sigma_2^{\alpha} + \delta_2^{\alpha} + \xi_1^{\alpha} + d^{\alpha}) I, \\ {}^{C}D^{\alpha}Q_2 &= \epsilon_2^{\alpha} Q_1 + \sigma_2^{\alpha} I - (\delta_3^{\alpha} + \xi_2^{\alpha} + d^{\alpha}) Q_2, \\ {}^{C}D^{\alpha}R &= \delta_1^{\alpha} Q_1 + \delta_2^{\alpha} I + \delta_3^{\alpha} Q_2 - d^{\alpha} R. \end{cases} \tag{2.1}$$

By summing the seven fractional-order differential equations and using

$$N = S + S_q + E + Q_1 + I + Q_2 + R,$$

one obtains the governing equation for the total population:

$${}^{C}D^{\alpha}N = \Lambda^{\alpha} - d^{\alpha}N - \xi_1^{\alpha}I - \xi_2^{\alpha}Q_2.$$

Thus, we obtain a Left-Caputo fractional derivative with fractional order $\alpha \in (0, 1]$.

The fractional-order epidemic model (2.1) describes the dynamics across seven compartments, including susceptible (S), susceptible with self-protective awareness (S_q), exposed (E), quarantined exposed (Q_1), infectious (I), quarantined infectious (Q_2), and recovered (R). Susceptible individuals become exposed through contact with infectious or exposed individuals and may move to quarantine. Exposed individuals transition to infectious or quarantined exposed states. Infectious individuals can recover, be quarantined, or die. The recovered population grows from recoveries in Q_1, I, and Q_2, while all compartments experience natural death. The total population N varies with population recruitment, natural mortality, and disease-induced mortality. All initial populations are assumed to be non-negative, i.e.,

$$S(0) \geq 0, \quad S_q(0) \geq 0, \quad E(0) \geq 0, \quad I(0) \geq 0, \quad Q_1(0) \geq 0, \quad Q_2(0) \geq 0, \quad R(0) \geq 0, \quad N(0) \geq 0.$$

Figure 1 presents a compartmental flow diagram of the fractional-order epidemic model. Susceptible individuals are recruited into the model at a constant Λ^{α}, and upon contact with either exposed or infectious individuals, they transition to the exposed compartment at the combined infection speed $(\beta_1^{\alpha}E + \beta_2^{\alpha}I)S$. A portion of susceptible individuals adopt protective behavior and move to S_q, while loss of that awareness causes them to return to S. Individuals in the exposed compartment are screened by nucleic acid testing at rate σ_1^{α} and transferred to Q_1, or they progress to the unprotected infectious compartment I at rate ε_1^{α}. Infectious individuals may recover from I to R at rate γ^{α} or die of disease at rate ξ_1^{α}; they may also be detected by nucleic acid testing at rate σ_2^{α} and moved to quarantine compartment Q_2. In compartments Q_1 and Q_2, individuals recover to R at rates δ_2^{α} and δ_3^{α}, while disease-induced mortality ξ_i^{α} $(i = 1, 2)$ during quarantine is also taken into account. Ultimately, all recovered individuals accumulate in R, and natural death at rate d^{α} leading to exit is considered in all compartments. This flow diagram clearly illustrates the dynamic mechanisms by which nucleic acid testing and protective behaviors operate across states.

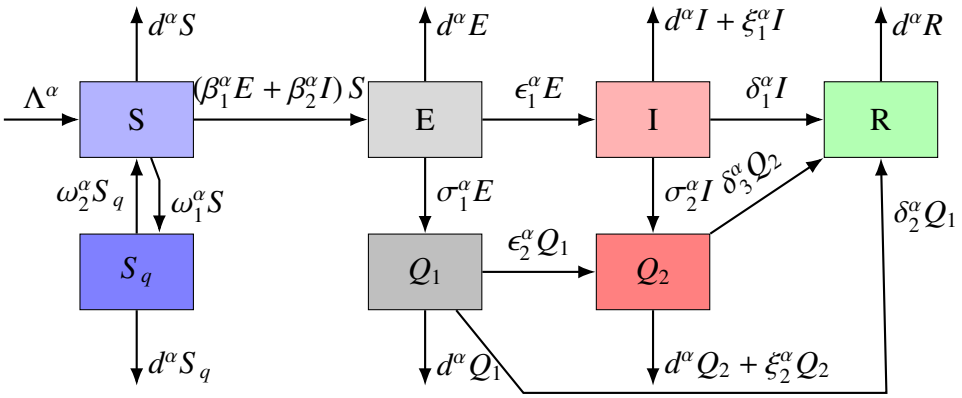

Figure 1. Compartment flow diagram of the fractional-order epidemic model.

3. Model analysis

In this section, we conduct a systematic and in-depth analysis of the dynamic behavior of model (2.1). First, by employing mathematical tools tailored to fractional-order differential equations, we prove the existence and uniqueness of solutions, and further show that solutions remain non-negative and bounded under non-negative initial conditions. Next, we apply the next-generation matrix method to derive the basic reproduction number R_0, analyzing from a biological perspective how each parameter influences the potential for an outbreak. We then provide comprehensive proofs for the existence and stability of both the DFE and the EE: For $R_0 < 1$, we first establish the local asymptotic stability of the DFE using the Jacobian matrix and the Routh-Hurwitz criteria, and subsequently prove its global asymptotic stability by constructing a suitable Lyapunov function and applying LaSalle's invariance principle; for $R_0 > 1$, under specific conditions, EE can be shown to be both locally and globally asymptotically stable. We also discuss the biological implications of these stability findings for epidemic control.

3.1. Existence, positivity, and boundedness of solutions

Theorem 1. *For any positive initial condition* $X(0) = (S(0), S_q(0), E(0), Q_1(0), I(0), Q_2(0), R(0)) \in \Gamma$, *there always exists a non-negative, bounded, and unique solution* $X(t) = (S(t), S_q(t), E(t), Q_1(t), I(t), Q_2(t), R(t)) \in \Gamma$ *for model* (2.1)*, and it remains in* $\mathbb{R}^7_+$, *where*

$$\Gamma = \left\{ X(t) \in \mathbb{R}^7_+ : 0 \le N = S + S_q + E + Q_1 + I + Q_2 + R \le \max\left\{ N(0), \frac{\Lambda^\alpha}{d^\alpha} \right\} \right\},$$

the closed set Γ *is the positive invariant of model* (2.1).

Proof of Theorem 1. To demonstrate the existence, nonnegativity, and boundedness of the solution to model (2.1), let the compartments corresponding to each of the equations in model (2.1) be 0. Specifically, due to the biological significance of each compartment, we have

$$S(0) \ge 0, \quad S_q(0) \ge 0, \quad E(0) \ge 0, \quad I(0) \ge 0, \quad Q_1(0) \ge 0, \quad Q_2(0) \ge 0, \quad R(0) \ge 0.$$

Under these conditions, we derive the following results:

$$\begin{aligned}
{}^C D^\alpha S|_{S=0} &= \Lambda^\alpha + \omega_2^\alpha S_q \ge 0,\\
{}^C D^\alpha S_q|_{S_q=0} &= \omega_1^\alpha S \ge 0,\\
{}^C D^\alpha E|_{E=0} &= \beta_2^\alpha S I \ge 0,\\
{}^C D^\alpha Q_1|_{Q_1=0} &= \sigma_1^\alpha E \ge 0,\\
{}^C D^\alpha I|_{I=0} &= \epsilon_1^\alpha E \ge 0,\\
{}^C D^\alpha Q_2|_{Q_2=0} &= \epsilon_2^\alpha Q_1 + \sigma_2^\alpha I \ge 0,\\
{}^C D^\alpha R|_{R=0} &= \delta_1^\alpha Q_1 + \delta_2^\alpha I + \delta_3^\alpha Q_2 \ge 0.
\end{aligned}$$

By using Theorem 2.1 in [37], we have $X(t) = (S(t), S_q(t), E(t), Q_1(t), I(t), Q_2(t), R(t)) \ge 0$ for any $t \ge 0$; thus, the nonnegativity of the solution is proved. Regarding the boundedness of the solutions, by adding the equations of model (2.1), we have

$${}^C D^\alpha N(t) = {}^C D^\alpha S(t) + {}^C D^\alpha S_q(t) + {}^C D^\alpha E(t) + {}^C D^\alpha Q_1(t) + {}^C D^\alpha I(t) + {}^C D^\alpha Q_2(t) + {}^C D^\alpha R(t)$$

$$= \Lambda^\alpha - d^\alpha S(t) - d^\alpha S_q(t) - d^\alpha E(t) - d^\alpha Q_1(t) - (d^\alpha + \xi_1^\alpha) I(t) - (d^\alpha + \xi_2^\alpha) Q_2(t) - d^\alpha R(t)$$
$$= \Lambda^\alpha - d^\alpha N(t) - \xi_1^\alpha I(t) - \xi_2^\alpha Q_2(t).$$

Since $I \geq 0, Q_2 \geq 0$, we obtain

$$^C D^\alpha N(t) \leq \Lambda^\alpha - d^\alpha N(t),$$

and from Lemma 3.3 in [38], we get

$$N(t) \leq \left[-\frac{\Lambda^\alpha}{d^\alpha} + N(0) \right] E_\alpha \left(-d^\alpha t^\alpha \right) + \frac{\Lambda^\alpha}{d^\alpha}.$$

If we take the limit as $t \to \infty$, $N \to \frac{\Lambda^\alpha}{d^\alpha}$, then we have

$$N(t) \leq \max \left\{ N(0), \frac{\Lambda^\alpha}{d^\alpha} \right\}.$$

This fact implies that S, S_q, E, Q_1, I, Q_2, R, and N are bounded. Then, we prove that model (2.1) with any positive initial condition has a unique solution. Model (2.1) can be rewritten as follows:

$$^C D^\alpha X(t) = A_1 X(t) + x_1(t) A_2 X(t) + \xi, \tag{3.1}$$

where

$$x_1(t) = S(t), \quad x_2(t) = S_q(t), \quad x_3(t) = E(t), \quad x_4(t) = Q_1(t),$$
$$x_5(t) = I(t), \quad x_6(t) = Q_2(t), \quad x_7(t) = R(t),$$

$$X = \begin{pmatrix} S \\ S_q \\ E \\ Q_1 \\ I \\ Q_2 \\ R \end{pmatrix}, \boldsymbol{\xi} = \begin{pmatrix} \Lambda^\alpha \\ 0 \\ 0 \\ 0 \\ 0 \\ 0 \\ 0 \end{pmatrix},$$

$$A_1 = \begin{pmatrix} -(\omega_1^\alpha + d^\alpha) & \omega_2^\alpha & 0 & 0 & 0 & 0 & 0 \\ \omega_1^\alpha & -(\omega_2^\alpha + d^\alpha) & 0 & 0 & 0 & 0 & 0 \\ 0 & 0 & -(\epsilon_1^\alpha + \sigma_1^\alpha + d^\alpha) & 0 & 0 & 0 & 0 \\ 0 & 0 & \sigma_1^\alpha & -(\epsilon_2^\alpha + \delta_1^\alpha + d^\alpha) & 0 & 0 & 0 \\ 0 & 0 & \epsilon_1^\alpha & 0 & -(\sigma_2^\alpha + \delta_2^\alpha + \xi_1^\alpha + d^\alpha) & 0 & 0 \\ 0 & 0 & 0 & \epsilon_2^\alpha & \sigma_2^\alpha & -(\delta_3^\alpha + \xi_2^\alpha + d^\alpha) & 0 \\ 0 & 0 & 0 & \delta_1^\alpha & \delta_2^\alpha & \delta_3^\alpha & -d^\alpha \end{pmatrix},$$

$$A_2 = \begin{pmatrix} 0 & 0 & -\beta_1^\alpha & 0 & -\beta_2^\alpha & 0 & 0 \\ 0 & 0 & \beta_1^\alpha & 0 & \beta_2^\alpha & 0 & 0 \\ 0 & 0 & 0 & 0 & 0 & 0 & 0 \\ 0 & 0 & 0 & 0 & 0 & 0 & 0 \\ 0 & 0 & 0 & 0 & 0 & 0 & 0 \\ 0 & 0 & 0 & 0 & 0 & 0 & 0 \\ 0 & 0 & 0 & 0 & 0 & 0 & 0 \end{pmatrix},$$

From Eq (3.1), we have

$$\|{}^{C}D^{\alpha}X\| \leq (\|A_1\| + \|A_2\|)\|X\|.$$

According to Lemma 2.1 in [39], we can get that there exists a unique solution for model (2.1) at any initial condition. In summary, the total population of our constructed model, $S + S_q + E + Q_1 + I + Q_2 + R$, is bounded by a boundedness, ensuring the boundedness of solutions. These results indicate that model (2.1) not only admits a unique solution for any initial condition but also, in a biological sense, keeps each compartment's population values reasonable (non-negative and bounded), thereby providing a theoretical foundation for subsequent stability analysis and numerical simulations. □

3.2. Basic reproduction number

The basic reproduction number R_0 is a core concept in infectious disease epidemiology. It represents the average number of susceptible individuals that one infected person can transmit the disease to during their infectious period. The value of R_0 directly reflects the potential for disease transmission and plays a critical role in predicting the course of an epidemic and in formulating control strategies. If $R_0 > 1$, it means that each infected individual will, on average, transmit the disease to more than one person, it suggests that the disease could spread within the population and potentially cause an outbreak. If $R_0 < 1$, the transmission of the disease will gradually decline, leading to its eradication [40]. We use the next-generation matrix method described in [41] to compute the basic reproduction number, as detailed below:

$$R_0 = \rho(FV^{-1}).$$

Here, ρ represents the largest eigenvalue or spectral radius, F is the non-negative matrix of new infection terms, and V is the non-singular matrix of the remaining transition terms. We use four compartments E, Q_1, I, Q_2. These two matrices are given as follows:

$$F = \begin{pmatrix} \beta_1^{\alpha} S^0 & 0 & \beta_2^{\alpha} S^0 & 0 \\ 0 & 0 & 0 & 0 \\ 0 & 0 & 0 & 0 \\ 0 & 0 & 0 & 0 \end{pmatrix},$$

$$V = \begin{pmatrix} \epsilon_1^{\alpha} + \sigma_1^{\alpha} + d^{\alpha} & 0 & 0 & 0 \\ -\sigma_1^{\alpha} & \epsilon_2^{\alpha} + \delta_1^{\alpha} + d^{\alpha} & 0 & 0 \\ -\epsilon_1^{\alpha} & 0 & \xi_1^{\alpha} + \delta_2^{\alpha} + \sigma_2^{\alpha} + d^{\alpha} & 0 \\ 0 & -\epsilon_2^{\alpha} & -\sigma_3^{\alpha} & \xi_2^{\alpha} + \delta_3^{\alpha} + d^{\alpha} \end{pmatrix}.$$

Then, we have

$$FV^{-1} = \begin{pmatrix} \frac{\beta_1^{\alpha} S^0}{d^{\alpha} + \epsilon_1^{\alpha} + \sigma_1^{\alpha}} + \frac{\epsilon_1^{\alpha} \beta_2^{\alpha} S^0}{(d^{\alpha} + \epsilon_1^{\alpha} + \sigma_1^{\alpha})(d^{\alpha} + \delta_2^{\alpha} + \xi_1^{\alpha} + \sigma_2^{\alpha})} & 0 & \frac{\beta_2^{\alpha} S_0}{d^{\alpha} + \delta_2^{\alpha} + \xi_1^{\alpha} + \sigma_2^{\alpha}} & 0 \\ 0 & 0 & 0 & 0 \\ 0 & 0 & 0 & 0 \\ 0 & 0 & 0 & 0 \end{pmatrix}.$$

The basic reproduction number R_0 for model (2.1) is determined by calculating the dominant

eigenvalue of the matrix product. It is expressed as

$$\begin{aligned} R_0 &= \rho(FV^{-1}) \\ &= \underbrace{\frac{\beta_1^\alpha S^0}{d+\epsilon_1^\alpha+\sigma_1^\alpha}}_{\text{Exposed contribution}} + \underbrace{\frac{\epsilon_1^\alpha\beta_2^\alpha S^0}{(d^\alpha+\epsilon_1^\alpha+\sigma_1^\alpha)(d^\alpha+\delta_2^\alpha+\xi_1^\alpha+\sigma_2^\alpha)}}_{\text{Infectious contribution}}, \end{aligned} \tag{3.2}$$

where the first term represents the contribution from the exposed class and the second term captures the contribution from the infectious class.

By substituting the equilibrium value of S^0, we obtain a more compact expression for R_0,

$$R_0 = \frac{\Lambda^\alpha(\omega_2^\alpha+d^\alpha)[\beta_1^\alpha(d^\alpha+\delta_2^\alpha+\xi_1^\alpha+\sigma_2^\alpha)+\epsilon_1^\alpha\beta_2^\alpha]}{d^\alpha(d^\alpha+\omega_1^\alpha+\omega_2^\alpha)(d^\alpha+\epsilon_1^\alpha+\sigma_1^\alpha)(d^\alpha+\delta_2^\alpha+\xi_1^\alpha+\sigma_2^\alpha)}. \tag{3.3}$$

Equation (3.3) combines the key factors of the basic reproduction number R_0 into two contributions: One from the exposed compartment and one directly from the infectious compartment. The term $\Lambda^\alpha(\omega_2^\alpha+d^\alpha)$, together with ω_1^α and ω_2^α, determines the initial susceptible population: Raising ω_1^α (greater protective awareness) reduces susceptibles and, hence, R_0, while increasing ω_2^α has the opposite effect. Inside the brackets, $\beta_1^\alpha(d^\alpha+\delta_2^\alpha+\xi_1^\alpha+\sigma_2^\alpha)$ captures "direct transmission after exposure" and $\varepsilon_1^\alpha\beta_2^\alpha$ captures "transmission after becoming infectious," where a higher σ_2^α leads to faster isolation and lowers transmission. The denominator consists of the rates at which individuals leave each stage, encompassing natural death, testing, isolation, and recovery. Self-protection (ω_1^α, ω_2^α) and testing (σ_1^α, σ_2^α) parameters work together to block transmission during both the exposed and infectious periods, determining whether the epidemic continues: If $R_0 < 1$, the outbreak cannot spread; and if $R_0 > 1$, there is a risk of epidemic expansion.

3.3. Equilibrium analysis

In epidemiological dynamic models, the DFE and the EE are critical concepts for understanding disease transmission and control. The DFE represents a state where the disease has been eradicated or has not entered the population; analyzing its stability assists in determining whether the disease will spread within the community and in formulating appropriate control strategies. The EE signifies a steady state where the disease persists in the population; thus, investigating its existence and stability can reveal the long-term dynamical behavior of the disease, thereby guiding resource allocation and the development of long-term control measures.

3.3.1. Existence and stability of the DFE

Theorem 2. *In model* (2.1)*, there always exists a DFE* $X^0 = \left(\frac{\Lambda^\alpha(\omega_2^\alpha+d^\alpha)}{d^\alpha(d^\alpha+\omega_1^\alpha+\omega_2^\alpha)}, \frac{\Lambda^\alpha\omega_1^\alpha}{d^\alpha(d^\alpha+\omega_1^\alpha+\omega_2^\alpha)}, 0, 0, 0, 0, 0\right)$.

Proof of Theorem 2. Since we are calculating the DFE, we consider the characteristics of the DFE in epidemiological dynamics. Letting $E^0 = 0$, $I^0 = 0$ in model (2.1), we obtain

$$S^0 = \frac{\Lambda^\alpha(\omega_2^\alpha+d^\alpha)}{d^\alpha(d^\alpha+\omega_1^\alpha+\omega_2^\alpha)}, \quad S_q^0 = \frac{\Lambda^\alpha\omega_1^\alpha}{d^\alpha(d^\alpha+\omega_1^\alpha+\omega_2^\alpha)}, \quad Q_1^0 = 0, \quad Q_2^0 = 0, \quad R^0 = 0.$$

Therefore, the DFE of model (2.1) is $X^0 = \left(\frac{\Lambda^\alpha(\omega_2^\alpha+d^\alpha)}{d^\alpha(d^\alpha+\omega_1^\alpha+\omega_2^\alpha)}, \frac{\Lambda^\alpha\omega_1^\alpha}{d^\alpha(d^\alpha+\omega_1^\alpha+\omega_2^\alpha)}, 0, 0, 0, 0, 0\right)$. It is straightforward to see that for model (2.1), there always exists a DFE X^0 that represents the ideal state after the outbreak has been completely cleared: No individuals remain in the exposed or infectious compartments, and the population resides in the two susceptible classes (S and S_q). At this equilibrium, the recruitment constant Λ^α, the natural death rate d^α, and the transition rates between "unprotected" (S) and "protective-awareness" (S_q) susceptibles (ω_1^α, ω_2^α) are in exact balance, so that S^0 and S_q^0 remain constant. Since $E = Q_1 = I = Q_2 = R = 0$, there is no risk of transmission. In the subsequent stability analysis, we investigate the conditions under which the system will spontaneously return to this DFE. □

Theorem 3. *The DFE X^0 of model* (2.1) *is locally asymptotically stable if the condition $R_0 < 1$ is satisfied.*

Proof of Theorem 3. The Jacobian matrix of model (2.1) at the DFE X^0 is given by:

$$J(X^0) = \begin{bmatrix} -d^\alpha-\omega_1^\alpha & \omega_2^\alpha & -\beta_1^\alpha S^0 & 0 & -\beta_2^\alpha S^0 & 0 & 0 \\ \omega_1^\alpha & -d^\alpha-\omega_2^\alpha & 0 & 0 & 0 & 0 & 0 \\ 0 & 0 & \beta_1^\alpha S^0 - d^\alpha - \epsilon_1^\alpha - \sigma_1 & 0 & \beta_2 S^0 & 0 & 0 \\ 0 & 0 & \sigma_1^\alpha & -d^\alpha-\delta_1^\alpha-\epsilon_2^\alpha & 0 & 0 & 0 \\ 0 & 0 & \epsilon_1^\alpha & 0 & -d^\alpha-\delta_2^\alpha-\xi_1^\alpha-\sigma_2^\alpha & 0 & 0 \\ 0 & 0 & 0 & \epsilon_2^\alpha & \sigma_2^\alpha & -d^\alpha-\delta_3^\alpha-\xi_2^\alpha & 0 \\ 0 & 0 & 0 & \delta_1^\alpha & \delta_2^\alpha & \delta_3^\alpha & -d^\alpha \end{bmatrix}.$$

Clearly, $-d^\alpha$, $-d^\alpha$, $(-d^\alpha-\delta_3^\alpha-\xi_2^\alpha)$, $(-d^\alpha-\delta_1^\alpha-\epsilon_2^\alpha)$, and $(-d^\alpha-\omega_1^\alpha-\omega_2^\alpha)$ are five eigenvalues of the matrix $J(X^0)$. For the other eigenvalues of the matrix $J(X^0)$, we have

$$J_1 = \begin{bmatrix} \beta_1^\alpha S^0 - d - \epsilon_1^\alpha - \sigma_1^\alpha & \beta_2^\alpha S^0 \\ \epsilon_1^\alpha & -d^\alpha-\delta_2^\alpha-\xi_1^\alpha-\sigma_2^\alpha \end{bmatrix}.$$

The characteristic equation is

$$\lambda^2 + c_1\lambda + c_2 = 0,$$

where

$$\begin{aligned} c_1 &= -\beta_1^\alpha S^0 + (d^\alpha+\epsilon_1^\alpha+\sigma_1^\alpha) + (d^\alpha+\delta_2^\alpha+\xi_1^\alpha+\sigma_2^\alpha), \\ c_2 &= (-\beta_1^\alpha S^0 + d^\alpha + \epsilon_1^\alpha + \sigma_1^\alpha)(d^\alpha+\delta_2^\alpha+\xi_1^\alpha+\sigma_2^\alpha) - \epsilon_1^\alpha\beta_2^\alpha S^0. \end{aligned}$$

Let the two eigenvalues be λ_1 and λ_2. The two eigenvalues satisfy the following conditions:

$$\begin{aligned} \lambda_1+\lambda_2 &= \beta_1^\alpha S^0 - (d^\alpha+\epsilon_1^\alpha+\sigma_1^\alpha) - (d^\alpha+\delta_2^\alpha+\xi_1^\alpha+\sigma_2^\alpha), \\ \lambda_1\lambda_2 &= (-\beta_1^\alpha S^0 + d^\alpha + \epsilon_1^\alpha + \sigma_1^\alpha)(d^\alpha+\delta_2^\alpha+\xi_1^\alpha+\sigma_2^\alpha) - \epsilon_1^\alpha\beta_2^\alpha S^0 \\ &= (d^\alpha+\epsilon_1^\alpha+\sigma_1^\alpha)(d^\alpha+\delta_2^\alpha+\xi_1^\alpha+\sigma_2^\alpha)(1-R_0). \end{aligned}$$

When $R_0 < 1$

$$\frac{\beta_1^\alpha S^0}{d^\alpha+\epsilon_1^\alpha+\sigma_1^\alpha} + \frac{\epsilon_1^\alpha\beta_2^\alpha S^0}{(d^\alpha+\epsilon_1^\alpha+\sigma_1^\alpha)(d^\alpha+\delta_2^\alpha+\xi_1^\alpha+\sigma_2^\alpha)} < 1,$$

$$\beta_1^\alpha S^0 + \frac{\epsilon_1^\alpha \beta_2^\alpha S^0}{d^\alpha + \delta_2^\alpha + \xi_1^\alpha + \sigma_2^\alpha} < d^\alpha + \epsilon_1^\alpha + \sigma_1^\alpha,$$
$$\beta_1^\alpha S^0 < d^\alpha + \epsilon_1^\alpha + \sigma_1^\alpha,$$
$$\beta_1^\alpha S^0 < (d^\alpha + \epsilon_1^\alpha + \sigma_1^\alpha) + (d^\alpha + \delta_2^\alpha + \xi_1^\alpha + \sigma_2^\alpha).$$

Thus, we have

$$\lambda_1 + \lambda_2 < 0,$$
$$\lambda_1 \lambda_2 > 0.$$

Therefore, $\lambda_1 < 0$, $\lambda_2 < 0$. By using the Routh-Hurwitz criterion [42], we can conclude that when $R_0 < 1$, the DFE is local asymptotic stability. This means that if a small number of exposed or infectious individuals are present in a community's initial state and the basic reproduction number $R_0 < 1$, the transmission chain will locally die out over time, and the system will spontaneously return to the DFE X^0, thereby ensuring that the epidemic cannot take off and spread widely. □

Theorem 4. *The DFE X^0 of model* (2.1) *is globally asymptotically stable if condition $R_0 < 1$ is satisfied.*

Proof of Theorem 4. Construct a Lyapunov function [43]:

$$L_1(t) = E + \frac{(d^\alpha + \epsilon_1^\alpha + \sigma_1^\alpha)}{\epsilon_1^\alpha} I.$$

Obviously $L_1(t) > 0$. Then, taking the partial derivative of the function yields

$$\begin{aligned}
{}^C D^\alpha L_1(t) &= \beta_1^\alpha S E + \beta_2^\alpha S I - (\epsilon_1^\alpha + \sigma_1^\alpha + d^\alpha)E + \frac{(d^\alpha + \epsilon_1^\alpha + \sigma_1^\alpha)}{\epsilon_1^\alpha}\left[\epsilon_1^\alpha E - (\sigma_2^\alpha + \delta_2^\alpha + \xi_1^\alpha + d^\alpha)I\right] \\
&= \beta_1^\alpha S E + \beta_2^\alpha S I - \frac{(d^\alpha + \epsilon_1^\alpha + \sigma_1^\alpha)(\sigma_2^\alpha + \delta_2^\alpha + \xi_1^\alpha + d^\alpha)}{\epsilon_1^\alpha} I \\
&= \beta_1^\alpha S \frac{\sigma_2^\alpha + \delta_2^\alpha + \xi_1^\alpha + d^\alpha}{\epsilon_1^\alpha} I + \beta_2^\alpha S I - \frac{(d^\alpha + \epsilon_1^\alpha + \sigma_1^\alpha)(\sigma_2^\alpha + \delta_2^\alpha + \xi_1^\alpha + d^\alpha)}{\epsilon_1^\alpha} I \\
&\leq \beta_1^\alpha S^0 \frac{\sigma_2^\alpha + \delta_2^\alpha + \xi_1^\alpha + d^\alpha}{\epsilon_1^\alpha} I + \beta_2^\alpha S^0 I - \frac{(d^\alpha + \epsilon_1^\alpha + \sigma_1^\alpha)(\sigma_2^\alpha + \delta_2^\alpha + \xi_1^\alpha + d^\alpha)}{\epsilon_1^\alpha} I \\
&= \frac{(d^\alpha + \epsilon_1^\alpha + \sigma_1^\alpha)(\sigma_2^\alpha + \delta_2^\alpha + \xi_1^\alpha + d^\alpha)}{\epsilon_1^\alpha} I \left[\frac{\beta_1^\alpha S^0}{d^\alpha + \epsilon_1^\alpha + \sigma_1^\alpha} + \frac{\epsilon_1^\alpha \beta_2^\alpha S^0}{(d^\alpha + \epsilon_1^\alpha + \sigma_1^\alpha)(d^\alpha + \delta_2^\alpha + \xi_1^\alpha + \sigma_2^\alpha)} - 1\right] \\
&= \frac{(d^\alpha + \epsilon_1^\alpha + \sigma_1^\alpha)(\sigma_2^\alpha + \delta_2^\alpha + \xi_1^\alpha + d^\alpha)}{\epsilon_1^\alpha} I(R_0 - 1).
\end{aligned}$$

When $R_0 < 1$, ${}^C D^\alpha L_1(t) < 0$, and ${}^C D^\alpha L_1(t) = 0$ if and only if $I = 0$. The maximum invariant set for $\{(S, S_q, E, Q_1, I, Q_2, R) \in \Gamma : {}^C D^\alpha L_1 = 0\}$ is the singleton $\{X^0\}$. According to LaSalle's invariance principle [44], X^0 is globally asymptotically stable. Thus, because the DFE is globally asymptotically stable, the system is not only locally stable under small perturbations but also converges globally for any initial number of exposed or infectious individuals. In other words, local stability guarantees only

that the system returns to the disease-free state when the number of infections is small; global stability, on the other hand, ensures that as long as $R_0 < 1$, no matter how many exposed or infectious individuals are initially present, the transmission chain will decay monotonically and the system will return to the disease-free equilibrium X^0. □

3.3.2. Existence and stability of the EE

Theorem 5. *There exists a unique EE* $X^* = (S^*, S_q^*, E^*, Q_1^*, I^*, Q_2^*, R^*)$ *in model* (2.1) *if it satisfies the condition* $R_0 > 1$.

Proof of Theorem 5. Based on the properties of the EE, setting the left-hand side of model (2.1) to zero, the point EE $X^* = (S^*, S_q^*, E^*, Q_1^*, I^*, Q_2^*, R^*)$ should satisfy the following equation:

$$\begin{cases} 0 &= \Lambda^\alpha + \omega_2^\alpha S_q^* - \beta_1^\alpha S^* E^* - \beta_2^\alpha S^* I^* - (\omega_1^\alpha + d^\alpha) S^*, \\ 0 &= \omega_1^\alpha S^* - (\omega_2^\alpha + d^\alpha) S_q^*, \\ 0 &= \beta_1^\alpha S^* E^* + \beta_2^\alpha S^* I^* - (\epsilon_1^\alpha + \sigma_1^\alpha + d^\alpha) E^*, \\ 0 &= \sigma_1^\alpha E^* - (\epsilon_2^\alpha + \delta_1^\alpha + d^\alpha) Q_1^*, \\ 0 &= \epsilon_1^\alpha E^* - (\sigma_2^\alpha + \delta_2^\alpha + \xi_1^\alpha + d^\alpha) I^*, \\ 0 &= \epsilon_2^\alpha Q_1^* + \sigma_2^\alpha I^* - (\delta_3^\alpha + \xi_2^\alpha + d^\alpha) Q_2^*, \\ 0 &= \delta_1^\alpha Q_1^* + \delta_2^\alpha I^* + \delta_3^\alpha Q_2^* - d^\alpha R^*. \end{cases} \tag{3.4}$$

Using compartments I to represent other compartments, we get

$$\begin{aligned} S^* &= \frac{(\epsilon_1^\alpha + \sigma_1^\alpha + d^\alpha) E^*}{\beta_1^\alpha E^* + \beta_2^\alpha I^*}, \\ S_q^* &= \frac{\omega_1^\alpha S^*}{\omega_2^\alpha + d^\alpha}, \\ E^* &= \frac{\sigma_2^\alpha + \delta_2^\alpha + \xi_1^\alpha + d^\alpha}{\epsilon_1^\alpha} I^*, \\ Q_1^* &= \frac{\sigma_1^\alpha}{\epsilon_2^\alpha + \delta_1^\alpha + d^\alpha} E^*, \\ I^* &= I^*, \\ Q_2^* &= \frac{\epsilon_2^\alpha Q_1^* + \sigma_2^\alpha I^*}{\delta_3^\alpha + \xi_2^\alpha + d^\alpha}, \\ R^* &= \frac{\delta_1^\alpha Q_1^* + \delta_2^\alpha I^* + \delta_3^\alpha Q_2^*}{d^\alpha}. \end{aligned}$$

Taking S^* and E^* into the first equation of Eq (3.4), we have

$$0 = \Lambda^\alpha + \frac{\omega_1^\alpha \omega_2^\alpha S^*}{\omega_2^\alpha + d^\alpha} - \frac{(\epsilon_1^\alpha + \sigma_1^\alpha + d^\alpha)(\sigma_2^\alpha + \delta_2^\alpha + \xi_1^\alpha + d^\alpha)}{\epsilon_1^\alpha} I^* - (\omega_1^\alpha + d^\alpha) S^*.$$

Thus,

$$I^* = \left(\Lambda^\alpha - \frac{(\omega_1^\alpha + \omega_2^\alpha + d^\alpha) d^\alpha}{\omega_2^\alpha + d^\alpha} S^* \right) \frac{(\epsilon_1^\alpha + \sigma_1^\alpha + d^\alpha)(\sigma_2^\alpha + \delta_2^\alpha + \xi_1^\alpha + d^\alpha)}{\epsilon_1^\alpha}$$

$$= \left(\Lambda^\alpha - \frac{(\omega_1^\alpha + \omega_2^\alpha + d^\alpha)d^\alpha}{\omega_2^\alpha + d^\alpha} \frac{(\epsilon_1^\alpha + \sigma_1^\alpha + d^\alpha)(\sigma_2^\alpha + \delta_2^\alpha + \xi_1^\alpha + d^\alpha)}{\beta_1^\alpha(\sigma_2^\alpha + \delta_2^\alpha + \xi_1^\alpha + d^\alpha) + \beta_2^\alpha \epsilon_1^\alpha}\right) \frac{(\epsilon_1^\alpha + \sigma_1^\alpha + d^\alpha)(\sigma_2^\alpha + \delta_2^\alpha + \xi_1^\alpha + d^\alpha)}{\epsilon_1^\alpha}$$
$$= \Lambda^\alpha \left(1 - \frac{1}{R_0}\right) \frac{(\epsilon_1^\alpha + \sigma_1^\alpha + d^\alpha)(\sigma_2^\alpha + \delta_2^\alpha + \xi_1^\alpha + d^\alpha)}{\epsilon_1^\alpha}.$$

When $R_0 > 1$, we have $I^* > 0$. Therefore, S^*, S_q^*, E^*, Q_1^*, Q_2^*, and R^* are all greater than zero. Hence, model (2.1) has a unique EE X^*. When the basic reproduction number $R_0 > 1$, each exposed and infectious individual generates, on average, more than one new infection in a fully susceptible population, indicating that the disease can sustain itself and spread. Under this condition, model (2.1) admits a unique EE $X^* = (S^*, S_q^*, E^*, Q_1^*, I^*, Q_2^*, R^*)$ where $E^* > 0$ and $I^* > 0$, signifying a persistent presence of exposed and infected individuals at equilibrium. All compartments have strictly positive values, meaning the epidemic does not die out but instead persists at a stable level: Some individuals remain exposed or infected (and subsequently detected and quarantined), while others remain susceptible or recovered. □

Theorem 6. *If $R_0 > 1$, the EE X^* of the model* (2.1) *is locally asymptotically stable, provided the following conditions are satisfied*

$$a_1 > 0,$$
$$a_4 > 0,$$
$$\Delta_2 = \begin{vmatrix} a_1 & a_3 \\ 1 & a_2 \end{vmatrix} = a_1 a_2 - a_3 > 0,$$
$$\Delta_3 = \begin{vmatrix} a_1 & a_3 & 0 \\ 1 & a_2 & a_4 \\ 0 & a_1 & a_3 \end{vmatrix} = a_1 a_2 a_3 - a_1^2 a_4 - a_3^2 > 0,$$

where

$$\begin{aligned}
a_1 &= (-\beta_1^\alpha S^* + m + n) + (\omega_2^\alpha + d^\alpha) + (p + \omega_1^\alpha + d^\alpha),\\
a_2 &= \beta_1^\alpha S^* p - \omega_1^\alpha \omega_2^\alpha + (m - \beta_1^\alpha S^*)n - \beta_2^\alpha S^* \epsilon_1^\alpha + (\omega_2^\alpha + d^\alpha)(-\beta_1^\alpha S^* + m + n)\\
&\quad + (-\beta_1^\alpha S^* + m + n)(p + \omega_1^\alpha + d^\alpha) + (p + \omega_1^\alpha + d^\alpha)(\omega_2^\alpha + d^\alpha),\\
a_3 &= \beta_1^\alpha S^* pn + \beta_2^\alpha S^* p\epsilon_1^\alpha + \beta_1^\alpha S^*(\omega_2^\alpha + d^\alpha) - \omega_1^\alpha \omega_2^\alpha(-\beta_1^\alpha S^* + m + n)\\
&\quad + (m - \beta_1^\alpha S^*)n(p + \omega_1^\alpha + d^\alpha) - \beta_2^\alpha S^* \epsilon_1^\alpha (p + \omega_1^\alpha + d^\alpha)\\
&\quad + (m - \beta_1^\alpha S^*)n(\omega_2^\alpha + d^\alpha) - \beta_2^\alpha S^* \epsilon_1^\alpha (\omega_2^\alpha + d^\alpha)\\
&\quad + (p + \omega_1^\alpha + d^\alpha)(\omega_2^\alpha + d^\alpha)(-\beta_1^\alpha S^* + m + n),\\
a_4 &= \beta_1^\alpha S^* n(\omega_2^\alpha + d^\alpha) + \beta_2^\alpha S^* \epsilon_1^\alpha (\omega_2^\alpha + d^\alpha) + (m - \beta_1^\alpha S^*)n - \beta_2^\alpha S^* \epsilon_1^\alpha\\
&\quad + (m - \beta_1^\alpha S^*)n(\omega_2^\alpha + d^\alpha)(p + \omega_1^\alpha + d^\alpha) - \beta_2^\alpha S^* \epsilon_1^\alpha (\omega_2^\alpha + d^\alpha)(p + \omega_1^\alpha + d^\alpha),\\
p &= \beta_1^\alpha E^* + \beta_2^\alpha I^*,\\
m &= \epsilon_1^\alpha + \sigma_1^\alpha + d^\alpha,\\
n &= \sigma_2^\alpha + \delta_2^\alpha + \xi_1^\alpha + d^\alpha.
\end{aligned}$$

Proof of Theorem 6. Here, the 1st, 2nd, 3rd, and 5th equations in model (2.1) are independent of the 4th, 6th, and 7th equations. Therefore, we first consider the following submodel:

$$\begin{cases} {}^{C}D^{\alpha}\bar{S} & = \Lambda^{\alpha} + \omega_2^{\alpha}\bar{S_q} - \beta_1^{\alpha}\bar{S}\,\bar{E} - \beta_2^{\alpha}\bar{S}\,\bar{I} - (\omega_1^{\alpha} + d^{\alpha})\bar{S}, \\ {}^{C}D^{\alpha}\bar{S_q} & = \omega_1^{\alpha}\bar{S} - (\omega_2^{\alpha} + d^{\alpha})\bar{S_q}, \\ {}^{C}D^{\alpha}\bar{E} & = \beta_1^{\alpha}\bar{S}\,\bar{E} + \beta_2^{\alpha}\bar{S}\,\bar{I} - (\epsilon_1^{\alpha} + \sigma_1^{\alpha} + d^{\alpha})\bar{E}, \\ {}^{C}D^{\alpha}\bar{I} & = \epsilon_1^{\alpha}\bar{E} - (\sigma_2^{\alpha} + \delta_2^{\alpha} + \xi_1^{\alpha} + d^{\alpha})\bar{I}. \end{cases} \tag{3.5}$$

We can see that the set

$$\Omega = \left\{ X(t) \in \mathbb{R}_+^7 : 0 \le \bar{N} = \bar{S} + \bar{S_q} + \bar{E} + \bar{I} \le \max\left\{ \bar{N}(0), \frac{\Lambda^{\alpha}}{d^{\alpha}} \right\} \right\},$$

is a positively invariant set of model (3.5). The point $\bar{X^0} = \left(\frac{\Lambda^{\alpha}(\omega_2^{\alpha}+d^{\alpha})}{d^{\alpha}(d^{\alpha}+\omega_1^{\alpha}+\omega_2^{\alpha})}, \frac{\Lambda^{\alpha}\omega_1^{\alpha}}{d^{\alpha}(d^{\alpha}+\omega_1^{\alpha}+\omega_2^{\alpha})}, 0, 0 \right)$ is the DFE, and the unique EE $\bar{X^*} = (\bar{S}^*, \bar{S_q}^*, \bar{E}^*, \bar{I}^*)$ of model (3.5) exists if and only if $R_0 > 1$, where

$$\bar{S}^* = S^*, \quad \bar{S_q^*} = S_q^*, \quad \bar{E}^* = E^*, \quad \bar{I}^* = I^*.$$

The Jacobian matrix of model (3.5) at the point $\bar{X^*}$ is

$$J(\bar{X^*}) = \begin{pmatrix} -\beta_1^{\alpha}\bar{E}^* - \beta_2^{\alpha}\bar{I}^* - (\omega_1^{\alpha} + d^{\alpha}) & \omega_2^{\alpha} & -\beta_1^{\alpha}\bar{S}^* & -\beta_2^{\alpha}\bar{S}^* \\ \omega_1^{\alpha} & -(\omega_2^{\alpha} + d^{\alpha}) & 0 & 0 \\ \beta_1^{\alpha}\bar{E}^* + \beta_2^{\alpha}\bar{I}^* & 0 & \beta_1^{\alpha}\bar{S}^* - (\epsilon_1^{\alpha} + \sigma_1^{\alpha} + d^{\alpha}) & \beta_2^{\alpha}\bar{S}^* \\ 0 & 0 & \epsilon_1^{\alpha} & -(\sigma_2^{\alpha} + \delta_2^{\alpha} + \xi_1^{\alpha} + d^{\alpha}) \end{pmatrix}.$$

Let

$$\begin{aligned} p &= \beta_1^{\alpha}\bar{E}^* + \beta_2^{\alpha}\bar{I}^*, \\ m &= \epsilon_1^{\alpha} + \sigma_1^{\alpha} + d^{\alpha}, \\ n &= \sigma_2^{\alpha} + \delta_2^{\alpha} + \xi_1^{\alpha} + d^{\alpha}, \end{aligned}$$

we have

$$J(\bar{X^*}) = \begin{pmatrix} -p - \omega_1^{\alpha} - d^{\alpha} & \omega_2^{\alpha} & -\beta_1^{\alpha}S^* & -\beta_2^{\alpha}S^* \\ \omega_1^{\alpha} & -\omega_2^{\alpha} + d^{\alpha} & 0 & 0 \\ p & 0 & \beta_1^{\alpha}S^* - m & \beta_2^{\alpha}S^* \\ 0 & 0 & \epsilon_1^{\alpha} & -n \end{pmatrix}.$$

The characteristic equation is

$$\lambda^4 + a_1\lambda^3 + a_2\lambda^2 + a_3\lambda + a_4 = 0,$$

where

$$\begin{aligned} a_1 &= (-\beta_1^{\alpha}S^* + m + n) + (\omega_2^{\alpha} + d^{\alpha}) + (p + \omega_1^{\alpha} + d^{\alpha}), \\ a_2 &= \beta_1^{\alpha}S^*p - \omega_1^{\alpha}\omega_2^{\alpha} + (m - \beta_1^{\alpha}S^*)n - \beta_2^{\alpha}S^*\epsilon_1^{\alpha} + (\omega_2^{\alpha} + d^{\alpha})(-\beta_1^{\alpha}S^* + m + n) \\ &\quad + (-\beta_1^{\alpha}S^* + m + n)(p + \omega_1^{\alpha} + d^{\alpha}) + (p + \omega_1^{\alpha} + d^{\alpha})(\omega_2^{\alpha} + d^{\alpha}), \\ a_3 &= \beta_1^{\alpha}S^*pn + \beta_2^{\alpha}S^*p\epsilon_1^{\alpha} + \beta_1^{\alpha}S^*(\omega_2^{\alpha} + d^{\alpha}) - \omega_1^{\alpha}\omega_2^{\alpha}(-\beta_1^{\alpha}S^* + m + n) \end{aligned}$$

$$
\begin{aligned}
&+ (m - \beta_1^\alpha S^*)n(p + \omega_1^\alpha + d^\alpha) - \beta_2^\alpha S^* \epsilon_1^\alpha (p + \omega_1^\alpha + d^\alpha) \\
&+ (m - \beta_1^\alpha S^*)n(\omega_2^\alpha + d^\alpha) - \beta_2^\alpha S^* \epsilon_1^\alpha (\omega_2^\alpha + d^\alpha) \\
&+ (p + \omega_1^\alpha + d^\alpha)(\omega_2^\alpha + d^\alpha)(-\beta_1^\alpha S^* + m + n), \\
a_4 = \beta_1^\alpha S^* n(\omega_2^\alpha + d^\alpha) &+ \beta_2^\alpha S^* \epsilon_1^\alpha (\omega_2^\alpha + d^\alpha) + (m - \beta_1^\alpha S^*)n - \beta_2^\alpha S^* \epsilon_1^\alpha \\
&+ (m - \beta_1^\alpha S^*)n(\omega_2^\alpha + d^\alpha)(p + \omega_1^\alpha + d^\alpha) - \beta_2^\alpha S^* \epsilon_1^\alpha (\omega_2^\alpha + d^\alpha)(p + \omega_1^\alpha + d^\alpha).
\end{aligned}
$$

By using the Routh–Hurwitz conditions for fractional-order differential equations [42], we can say that the EE $\bar{X}^* = (\bar{S}^*, \bar{S_q}^*, \bar{E}^*, \bar{I}^*)$ is locally asymptotically stable, provided the following conditions are satisfied:

$$
\begin{aligned}
\Delta_1 &= \left|a_1\right| = a_1 > 0, \\
\Delta_2 &= \begin{vmatrix} a_1 & a_3 \\ 1 & a_2 \end{vmatrix} = a_1 a_2 - a_3 > 0, \\
\Delta_3 &= \begin{vmatrix} a_1 & a_3 & 0 \\ 1 & a_2 & a_4 \\ 0 & a_1 & a_3 \end{vmatrix} = a_1 a_2 a_3 - a_1^2 a_4 - a_3^2 > 0, \\
\Delta_4 &= \begin{vmatrix} a_1 & a_3 & 0 & 0 \\ 1 & a_2 & a_4 & 0 \\ 0 & a_1 & a_3 & 0 \\ 0 & 0 & a_2 & a_4 \end{vmatrix} = a_4 \Delta_3 > 0.
\end{aligned}
$$

As $t \to \infty$, the compartments (S, S_q, E, I) converge to (S^*, S_q^*, E^*, I^*), and the limiting system for the 4th, 6th, and 7th equations of model (2.1) is

$$
\begin{cases}
{}^C D^\alpha Q_1 &= \sigma_1^\alpha E^* - (\epsilon_2^\alpha + \delta_1^\alpha + d^\alpha) Q_1^*, \\
{}^C D^\alpha Q_2 &= \epsilon_2^\alpha Q_1^* + \sigma_2^\alpha I^* - (\delta_3^\alpha + \xi_2^\alpha + d^\alpha) Q_2^*, \\
{}^C D^\alpha R &= \delta_1^\alpha Q_1^* + \delta_2^\alpha I^* + \delta_3^\alpha Q_2^* - d^\alpha R^*.
\end{cases} \tag{3.6}
$$

In the limit, as $t \to \infty$, we have

$$
\begin{aligned}
Q_1^* &= \frac{\sigma_1^\alpha}{\epsilon_2^\alpha + \delta_1^\alpha + d^\alpha} E^*, \\
Q_2^* &= \frac{\epsilon_2^\alpha Q_1^* + \sigma_2^\alpha I^*}{\delta_3^\alpha + \xi_2^\alpha + d^\alpha}, \\
R^* &= \frac{\delta_1^\alpha Q_1^* + \delta_2^\alpha I^* + \delta_3^\alpha Q_2^*}{d^\alpha}.
\end{aligned}
$$

Thus, when the above conditions are satisfied, the endemic equilibrium $X^* = (S^*, S_q^*, E^*, Q_1^*, I^*, Q_2^*, R^*)$ of model (2.1) is locally asymptotically stable. Biologically, this means that if the disease has settled into a stable endemic state within the community, minor disturbances will not eliminate it; the infection will persist and quickly revert to the same prevalence level, making it difficult to eradicate through weak or transient interventions. □

Theorem 7. *If $R_0 > 1$ and the following inequalities hold:*

$$-1 + \frac{S^*}{S} + \frac{S_q}{S_q^*} - \frac{S_q S^*}{S_q^* S} \leq 0, \qquad 1 - \frac{R^*}{R} + \frac{Q_2}{Q_2^*} - \frac{R^* Q_2}{R Q_2^*} \leq 0,$$

$$\frac{S}{S^*} - \frac{S_q^* S}{S_q S^*} - \frac{S_q}{S_q^*} + 1 \leq 0, \quad \frac{I S}{I^* S^*} - \frac{E I S}{E^* I^* S^*} + 1 - \frac{E}{E^*} \leq 0,$$

then the EE X^* of model (2.1) *is globally asymptotically stable.*

Proof of Theorem 7. Define the Lyapunov function [45,46] as follows:

$$L_2(t) = \sum_{\Phi \in \{S, S_q, E, Q_1, I, Q_2, R\}} [\Phi - \Phi^* - \Phi^* \ln \tfrac{\Phi}{\Phi^*}].$$

According to Lemma IV.2 [47], we get

$${}^C D^\alpha L_2(t) \leq \sum_{\Phi} \left(1 - \tfrac{\Phi^*}{\Phi}\right) {}^C D^\alpha \Phi.$$

Expanding yields

$$\begin{aligned}
{}^C D^\alpha L_2(t) \leq & \left(1 - \tfrac{S^*}{S}\right) {}^C D^\alpha S + \left(1 - \tfrac{S_q^*}{S_q}\right) {}^C D^\alpha S_q + \left(1 - \tfrac{E^*}{E}\right) {}^C D^\alpha E \\
& + \left(1 - \tfrac{Q_1^*}{Q_1}\right) {}^C D^\alpha Q_1 + \left(1 - \tfrac{I^*}{I}\right) {}^C D^\alpha I + \left(1 - \tfrac{Q_2^*}{Q_2}\right) {}^C D^\alpha Q_2 + \left(1 - \tfrac{R^*}{R}\right) {}^C D^\alpha R \\
\leq & \left(1 - \tfrac{S^*}{S}\right)[\Lambda^\alpha + \omega_2^\alpha S_q - \beta_1^\alpha S E - \beta_2^\alpha S I - (\omega_1^\alpha + d^\alpha) S] \\
& + \left(1 - \tfrac{S_q^*}{S_q}\right)[\omega_1^\alpha S - (\omega_2^\alpha + d^\alpha) S_q] \\
& + \left(1 - \tfrac{E^*}{E}\right)[\beta_1^\alpha S E + \beta_2^\alpha S I - (\epsilon_1^\alpha + \sigma_1^\alpha + d^\alpha) E] \\
& + \left(1 - \tfrac{Q_1^*}{Q_1}\right)[\sigma_1^\alpha E - (\epsilon_2^\alpha + \delta_1^\alpha + d^\alpha) Q_1] \\
& + \left(1 - \tfrac{I^*}{I}\right)[\epsilon_1^\alpha E - (\sigma_2^\alpha + \delta_2^\alpha + \lambda_1^\alpha + d^\alpha) I] \\
& + \left(1 - \tfrac{Q_2^*}{Q_2}\right)[\epsilon_2^\alpha Q_1 + \sigma_2^\alpha I - (\delta_3^\alpha + \lambda_2^\alpha + d^\alpha) Q_2] \\
& + \left(1 - \tfrac{R^*}{R}\right)[\delta_1^\alpha Q_1 + \delta_2^\alpha I + \delta_3^\alpha Q_2 - d^\alpha R].
\end{aligned}$$

Then, we have

$$\begin{aligned}
\left(1 - \tfrac{S^*}{S}\right) {}^C D^\alpha S &= \left(1 - \tfrac{S^*}{S}\right)[\Lambda^\alpha + \omega_2^\alpha S_q - \beta_1^\alpha S E - \beta_2^\alpha S I - (\omega_1^\alpha + d^\alpha) S] \\
&= \omega_2^\alpha S_q^* \left(-1 + \tfrac{S^*}{S} + \tfrac{S_q}{S_q^*} - \tfrac{S_q S^*}{S_q^* S}\right) + \beta_1^\alpha S^* E^* \left(1 - \tfrac{S^*}{S} - \tfrac{E S}{E^* S^*} + \tfrac{E}{E^*}\right) \\
&\quad + \beta_2^\alpha S^* I^* \left(1 - \tfrac{S^*}{S} - \tfrac{I S}{I^* S^*} + \tfrac{I}{I^*}\right) + (\omega_1^\alpha + d^\alpha) S^* \left(2 - \tfrac{S}{S^*} - \tfrac{S^*}{S}\right), \\
\left(1 - \tfrac{S_q^*}{S_q}\right) {}^C D^\alpha S_q &= \left(1 - \tfrac{S_q^*}{S_q}\right)[\omega_1^\alpha S - (\omega_2^\alpha + d^\alpha) S_q] \\
&= (\omega_2^\alpha + d^\alpha) S_q^* \left(\tfrac{S}{S^*} - \tfrac{S_q^* S}{S_q S^*} - \tfrac{S_q}{S_q^*} + 1\right), \\
\left(1 - \tfrac{E^*}{E}\right) {}^C D^\alpha E &= \left(1 - \tfrac{E^*}{E}\right)[\beta_1^\alpha S E + \beta_2^\alpha S I - (\epsilon_1^\alpha + \sigma_1^\alpha + d^\alpha) E]
\end{aligned}$$

$$= \beta_1^\alpha S^* E^* \left(\frac{ES}{E^*S^*} - \frac{S}{S^*} - \frac{E}{E^*} + 1\right) + \beta_2^\alpha S^* I^* \left(\frac{IS}{I^*S^*} - \frac{EIS}{E^*I^*S^*} + 1 - \frac{E}{E^*}\right),$$

$$\left(1 - \frac{Q_1^*}{Q_1}\right) {}^C D^\alpha Q_1 = \left(1 - \frac{Q_1^*}{Q_1}\right)\left[\sigma_1^\alpha E - (\epsilon_2^\alpha + \delta_1^\alpha + d^\alpha) Q_1\right]$$
$$= (\epsilon_2^\alpha + \delta_1^\alpha + d^\alpha)\, Q_1^* \left(\frac{E}{E^*} - \frac{E\, Q_1^*}{E^*\, Q_1} - \frac{Q_1}{Q_1^*} + 1\right),$$

$$\left(1 - \frac{I^*}{I}\right) {}^C D^\alpha I = \left(1 - \frac{I^*}{I}\right)\left[\epsilon_1^\alpha E - (\sigma_2^\alpha + \delta_2^\alpha + \xi_1^\alpha + d^\alpha) I\right]$$
$$= (\sigma_2^\alpha + \delta_2^\alpha + \xi_1^\alpha + d^\alpha)\, I^* \left(\frac{E}{E^*} - \frac{E\, I^*}{E^*\, I} - \frac{I}{I^*} + 1\right),$$

$$\left(1 - \frac{Q_2^*}{Q_2}\right) {}^C D^\alpha Q_2 = \left(1 - \frac{Q_2^*}{Q_2}\right)\left[\epsilon_2^\alpha Q_1 + \sigma_2^\alpha I - (\delta_3^\alpha + \xi_2^\alpha + d^\alpha) Q_2\right]$$
$$= \epsilon_2^\alpha\, Q_1^* \left(1 + \frac{Q_1}{Q_1^*} - \frac{Q_1\, Q_2^*}{Q_1^*\, Q_2} - \frac{Q_2}{Q_2^*}\right) + \sigma_2^\alpha\, I^* \left(1 + \frac{I}{I^*} - \frac{I\, Q_2^*}{I^*\, Q_2} - \frac{Q_2}{Q_2^*}\right),$$

$$\left(1 - \frac{R^*}{R}\right) {}^C D^\alpha R = \left(1 - \frac{R^*}{R}\right)\left[\delta_1^\alpha Q_1 + \delta_2^\alpha I + \delta_3^\alpha Q_2 - d^\alpha R\right]$$
$$= \delta_1^\alpha\, Q_1^* \left(1 - \frac{R}{R^*} + \frac{Q_1}{Q_1^*} - \frac{R^*\, Q_1}{R\, Q_1^*}\right) + \delta_2^\alpha\, I^* \left(1 - \frac{R}{R^*} + \frac{I}{I^*} - \frac{R^*\, I}{R\, I^*}\right)$$
$$+ \delta_3^\alpha\, Q_2^* \left(1 - \frac{R^*}{R} + \frac{Q_2}{Q_2^*} - \frac{R^*\, Q_2}{R\, Q_2^*}\right).$$

By applying the arithmetic–geometric mean relation [48], we immediately obtain

$$1 - \frac{S^*}{S} - \frac{E\, S}{E^*\, S^*} + \frac{E}{E^*} \le 0, \quad 1 - \frac{S^*}{S} - \frac{I\, S}{I^*\, S^*} + \frac{I}{I^*} \le 0,$$

$$2 - \frac{S}{S^*} - \frac{S^*}{S} \le 0, \quad \frac{E\, S}{E^*\, S^*} - \frac{S}{S^*} - \frac{E}{E^*} + 1 \le 0,$$

$$\frac{E}{E^*} - \frac{E\, Q_1^*}{E^*\, Q_1} - \frac{Q_1}{Q_1^*} + 1 \le 0, \quad \frac{E}{E^*} - \frac{E\, I^*}{E^*\, I} - \frac{I}{I^*} + 1 \le 0,$$

$$1 + \frac{Q_1}{Q_1^*} - \frac{Q_1\, Q_2^*}{Q_1^*\, Q_2} - \frac{Q_2}{Q_2^*} \le 0, \quad 1 + \frac{I}{I^*} - \frac{I\, Q_2^*}{I^*\, Q_2} - \frac{Q_2}{Q_2^*} \le 0,$$

$$1 - \frac{R}{R^*} + \frac{Q_1}{Q_1^*} - \frac{R^*\, Q_1}{R\, Q_1^*} \le 0, \quad 1 - \frac{R}{R^*} + \frac{I}{I^*} - \frac{R^*\, I}{R\, I^*} \le 0.$$

The following inequalities must be satisfied to ensure the conditions hold:

$$-1 + \frac{S^*}{S} + \frac{S_q}{S_q^*} - \frac{S_q S^*}{S_q^* S} \le 0, \quad 1 - \frac{R^*}{R} + \frac{Q_2}{Q_2^*} - \frac{R^* Q_2}{R Q_2^*} \le 0,$$

$$\frac{S}{S^*} - \frac{S_q^* S}{S_q S^*} - \frac{S_q}{S_q^*} + 1 \le 0, \quad \frac{IS}{I^* S^*} - \frac{EIS}{E^* I^* S^*} + 1 - \frac{E}{E^*} \le 0.$$

We obtain ${}^C D^\alpha L_2(t) \le 0$. We then have ${}^C D^\alpha L_2(t) = 0$ if and only if $S = S^*$, $S_q = S_q^*$, $E = E^*$, $Q_1 = Q_1^*$, $I = I^*$, $Q_2 = Q_2^*$, and $R = R^*$. By LaSalle's invariance principle [44], the EE is globally asymptotically stable whenever $R_0 > 1$ and the above four inequalities are satisfied. This completes the proof of Theorem 7. □

From a biological perspective, when the basic reproduction number $R_0 > 1$, the epidemic will evolve and stabilize at the same endemic level regardless of how many exposed or infectious individuals

are initially present in the community. Even temporary fluctuations in testing, isolation, or protective awareness will not permanently alter the system; it will spontaneously return to that endemic state. In other words, the EE acts as an unavoidable "attractor" in the community, and only substantial changes in key parameters (for example, drastically increasing testing, isolation, or protective awareness to drive R_0 below 1) can move the epidemic away from this equilibrium and toward a disease-free state.

4. Numerical simulation

To verify the reliability of Theorems 1–7, and to confirm the roles of nucleic acid testing and individual protective awareness in epidemic control, we apply the PECE method from the ABM scheme [31] and use MATLAB R2022b to conduct numerical simulations under various conditions. This integrator uses carefully designed convolution-type weights to combine all past states in order to precisely capture the nonlocal memory characteristic of Caputo derivatives, achieving global convergence of approximately order $1 + \alpha$. Concretely, in the predict stage, the algorithm employs an explicit Adams–Bashforth scheme with fractional-order weights to generate an initial estimate at the next time point, fully leveraging historical data; then, during the first evaluation, this predicted value is used to approximate the derivative; in the correct stage, the method uses an implicit Adams–Moulton correction to iteratively refine that approximation by combining it with all past derivative values, yielding a more accurate corrected result that significantly improves precision and affords stiffness handling and remains stable even during long-term simulations or when the system becomes stiff; finally, in the second evaluation, the corrected value is again used to compute the derivative for the next iteration. Because this method applies weights based on the time intervals between past instants and the current instant at each step, it fully reproduces the "long-tail" memory effect of fractional-order models [49]. The hardware and software environment for these numerical simulations is presented in Table 2.

Table 2. Numerical simulation hardware and software environment.

Category	**Details**
Processor	12th Gen Intel Core i5-12500H @ 3.1GHz
GPU	NVIDIA GeForce RTX 3050 Laptop GPU (4GB GDDR6)
Operating System	Windows 11 Home 64-bit
Memory	16 GB DDR5-4800 (8GB x 2)
Storage	512 GB SSD (WD PC SN735)
MATLAB Version	MATLAB R2022b

Condition 1: $R_0 < 1$ (DFE). Given the following initial parameter values: $\beta_1 = 0.00008$, $\beta_2 = 0.00009$, $\omega_1 = 0.04$, $\omega_2 = 0.01$, $\sigma_1 = 0.01$, $\sigma_2 = 0.01$, $\epsilon_1 = 0.2$, $\epsilon_2 = 0.2$, $\xi_1 = 0.5$, $\xi_2 = 0.3$, $\delta_1 = 0.8$, $\delta_2 = 0.8$, $\delta_3 = 0.8$, $\Lambda = 10$, and $d = 0.01$, then the initial values for each compartment is $X(0) = (20000, 0, 1, 0, 1, 0, 0)$. In numerical simulations of fractional differential equations, reducing the order α extends the memory length, sharply increasing computational and storage demands while reducing solution smoothness and amplifying error accumulation. Predictor-corrector multi-step schemes are highly sensitive to the time step: Smaller α requires a finer step size to preserve stability; otherwise, oscillation or divergence may occur. A lower α also slows

convergence and degrades accuracy, making reliable results harder to achieve with fixed resources [49, 50]. Therefore, we choose α to be $(0.80, 0.85, 0.9, 0.95, 1.0)$. By calculation, we obtain that $R_0 = [0.1951, 0.1811, 0.1675, 0.1544, 0.1419]$ for different α. Through numerical simulation, we have Figure 2.

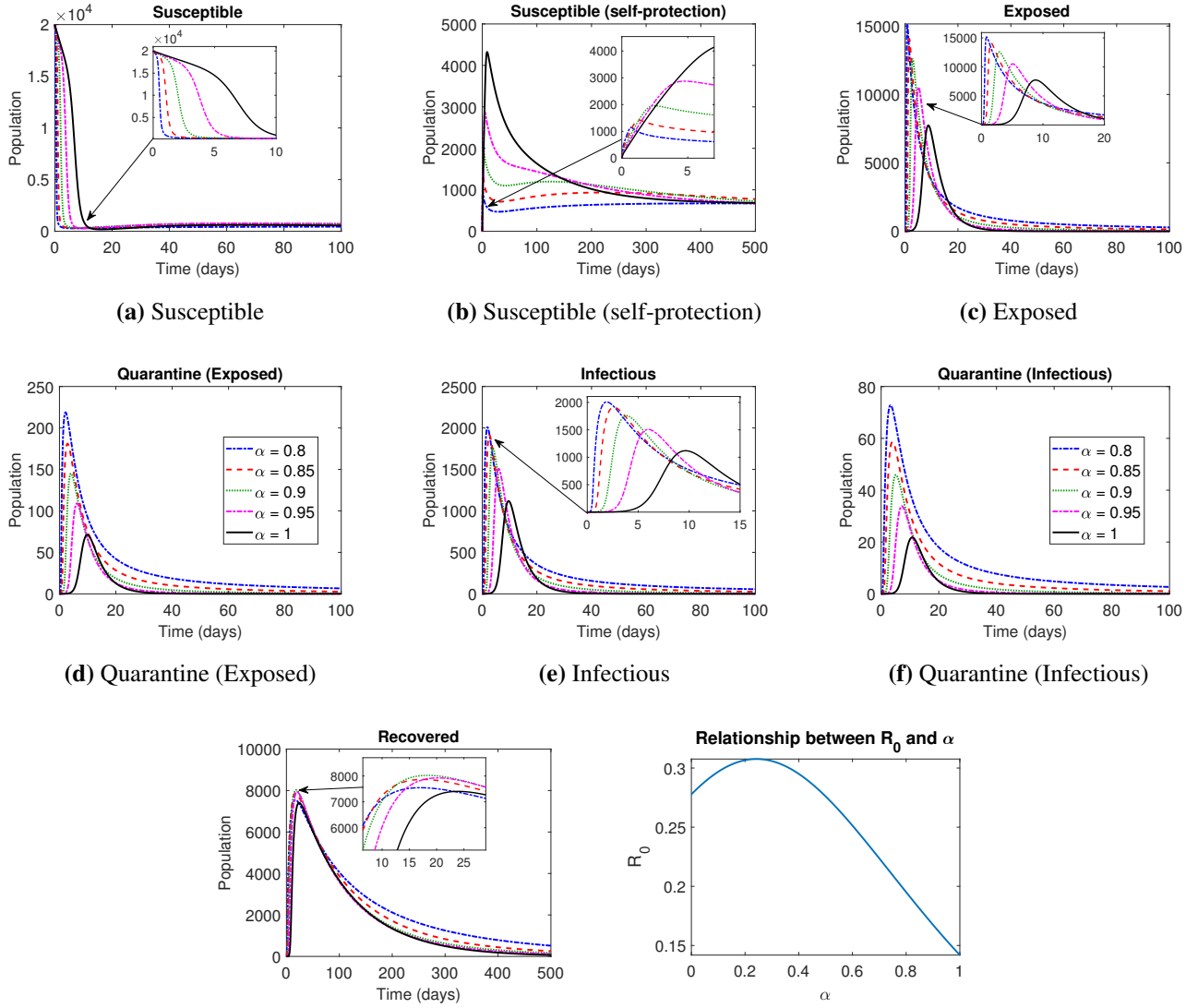

(a) Susceptible **(b)** Susceptible (self-protection) **(c)** Exposed

(d) Quarantine (Exposed) **(e)** Infectious **(f)** Quarantine (Infectious)

(g) Recovered **(h)** Relationship between R_0 and α

Figure 2. Epidemiological dynamics of the seven compartments and relationship between R_0 and α. Here, $R_0 < 1$.

From Figure 2, it can be observed that under the condition $R_0 < 1$, the population in each compartment initially undergoes rapid changes before gradually stabilizing over time. The number of susceptible individuals decreases significantly in the short term, while the number of exposed and infected individuals also declines rapidly due to isolation and treatment measures, indicating that the epidemic spread is effectively controlled. Moreover, the number of recovered individuals continuously increases, and the model reaches a stable state. This suggests that under the current parameter settings, the epidemic remains within a controllable range, further confirming the validity of Theorems 3 and 4.

It is worth noting that when α is small, the fractional derivative's memory effect is strongest, and all transmission and transition rates in the model are raised to the power of α. In this regime, terms such as β_i^α exceed their integer-order counterparts, causing early amplification of exposed and infected compartments and resulting in a higher, more rapidly occurring infection peak. Conversely, as α approaches 1, the model converges toward a classical first-order differential behavior, with diminished dependence on past states and α-powered parameters approaching their original values. Consequently, the accumulation of exposed and infected individuals slows down, the peak height decreases, and the decline from the peak to equilibrium becomes smoother, enabling the system to settle into a steady state more quickly.

Figure 2h shows that as α increases, R_0 first rises and then falls, indicating that the transmission characteristics of the epidemic change with different values of α. This behavior can be explained by Eq (3.3): When α is small, the growth effect induced by Λ^α dominates, causing R_0 to increase initially; as α grows further, all parameters less than 1 decay more rapidly when raised to the power α, which makes the combinations in both the numerator and denominator shrink quickly, and the denominator's overall rate of reduction eventually surpasses the numerator's growth. Consequently, R_0 decreases as α continues to increase.

Condition 2: $R_0 > 1$ (EE). $\beta_1 = 0.000008, \beta_2 = 0.000009, \omega_1 = 0.0004, \omega_2 = 0.0001, \sigma_1 = 0.1, \sigma_2 = 0.1, \epsilon_1 = 0.02, \epsilon_2 = 0.02, \xi_1 = 0.038, \xi_2 = 0.01, \delta_1 = 0.4, \delta_2 = 0.4, \delta_3 = 0.4, \Lambda = 5000, d = 0.01, X(0) = (20000, 0, 1, 0, 1, 0, 0)$, and α have different values $(0.80, 0.85, 0.9, 0.95, 1.0)$. By calculation, $R_0 = [13.2214, 16.3962, 20.2805, 25.0251, 30.8123]$. Through numerical simulation, we have Figure 3.

Figure 3 shows that when $R_0 > 1$, the disease continues to spread within the population and evolves into an endemic state. When the fractional order α is small, terms such as β_i^α are effectively amplified, and the memory effect of the fractional derivative is stronger. As a result, the exposed compartment E rapidly accumulates early on and quickly reaches a peak, which in turn drives the infected compartment I to exhibit an earlier peak. Moreover, the removal term $\epsilon_1^\alpha + \sigma_1^\alpha + d^\alpha$ is larger when $\alpha < 1$, causing E and I to decline swiftly after their peaks and move toward equilibrium. As α approaches 1, β_i^α and ϵ_1^α revert to their smaller original values; combined with the chosen initial conditions, this shift delays and raises the peak of E, consequently, I also peaks later and higher, with a more gradual post peak decay. The other compartments quarantine of exposed Q_1, quarantine of infected Q_2, and recovered R follow a similar pattern: for smaller α, peaks occur earlier and at lower heights and decay rapidly; for larger α, peaks occur later and at greater heights and decay more slowly. Ultimately, all compartments stabilize at a nonzero endemic equilibrium (EE), and that equilibrium level increases significantly with α. This demonstrates that α not only governs the height and timing of the epidemic peaks but also determines the final scale of the endemic state. Therefore, under the current parameter settings, the epidemic has indeed become endemic, confirming the validity of Theorems 6 and 7.

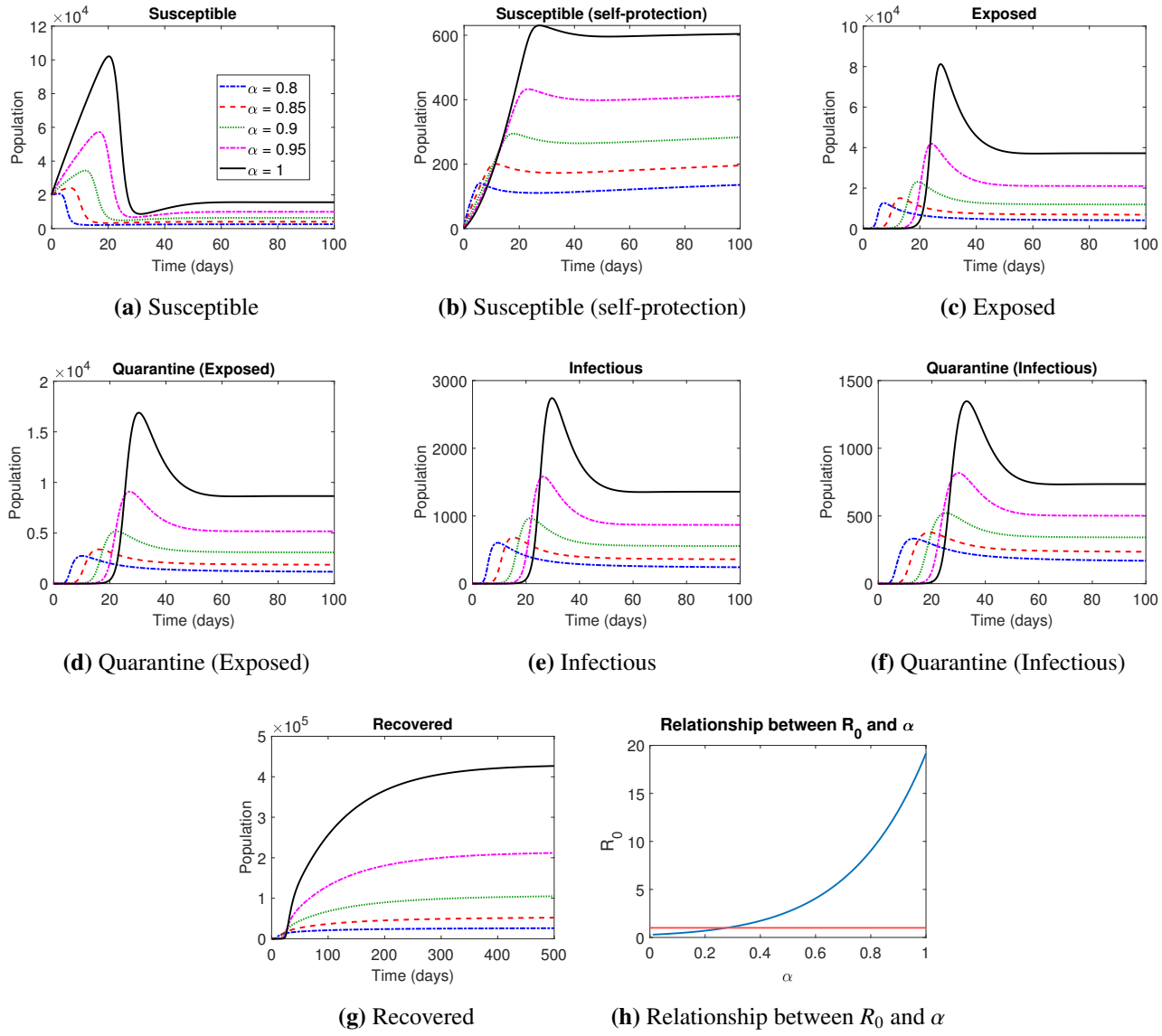

(a) Susceptible **(b)** Susceptible (self-protection) **(c)** Exposed

(d) Quarantine (Exposed) **(e)** Infectious **(f)** Quarantine (Infectious)

(g) Recovered **(h)** Relationship between R_0 and α

Figure 3. Epidemiological dynamics of the seven compartments and relationship between R_0 and α. Here, $R_0 > 1$.

Figure 3h shows that as α increases, the only parameter greater than one, Λ^{α}, begins to grow rapidly, while all other parameters less than 1 (such as β_i, ϵ_i, ω_i, and d) decrease when raised to the power of α. As a result, the numerator of $R_0(\alpha)$ steadily increases while the denominator steadily decreases, causing $R_0(\alpha)$ to rise at an accelerating pace. The red horizontal line at $R_0 = 1$ marks the epidemic threshold: Once α crosses approximately 0.3, R_0 exceeds 1, indicating that the disease shifts from likely dying out to likely persisting and becoming endemic. Therefore, variations in α not only affect the magnitude of R_0 but also directly determine whether the disease can persist in the population over the long term.

Condition 3: Different initial conditions. Under the parameter values $\alpha = 0.8$, $\beta_1 = 0.000008$, $\beta_2 = 0.000008$, $\omega_1 = 0.4$, $\omega_2 = 0.4$, $\sigma_1 = 0.001$, $\sigma_2 = 0.001$, $\epsilon_1 = 0.2$, $\epsilon_2 = 0.2$, $\xi_1 = 0.038$, $\xi_2 = 0.01$, $\delta_1 = 0.5$, $\delta_2 = 0.5$, $\delta_3 = 0.5$, $\Lambda = 1$, $d = 0.001$, and $\alpha = 0.85$, and with different initial values $X(0)$

($R_0 = 0.742 < 1$), the numerical simulation shows that the system converges to the DFE, as illustrated in Figure 4. Subsequently, we conduct simulations using the initial parameters from **Condition 2** (α is fixed at 0.8, $R_0 = 13.221 > 1$), and obtain Figure 5, where the system converges to the EE. These results demonstrate that variations in the initial value $X(0)$ do not affect the existence and stability of the solution, thereby verifying Theorem 1.

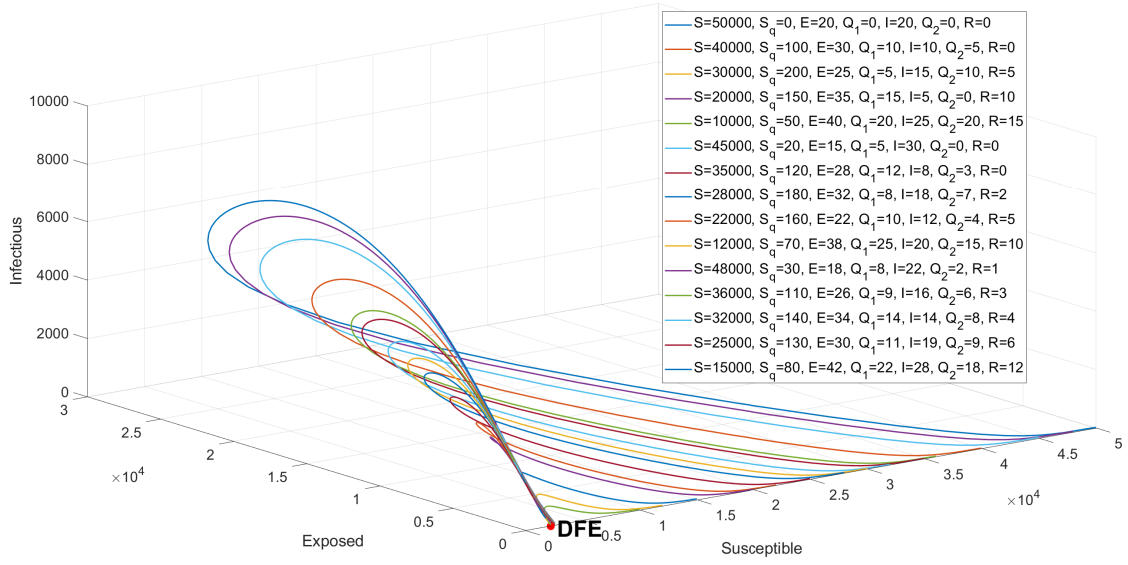

Figure 4. System trajectories under Condition 3 ($R_0 < 1$), converging to the DFE.

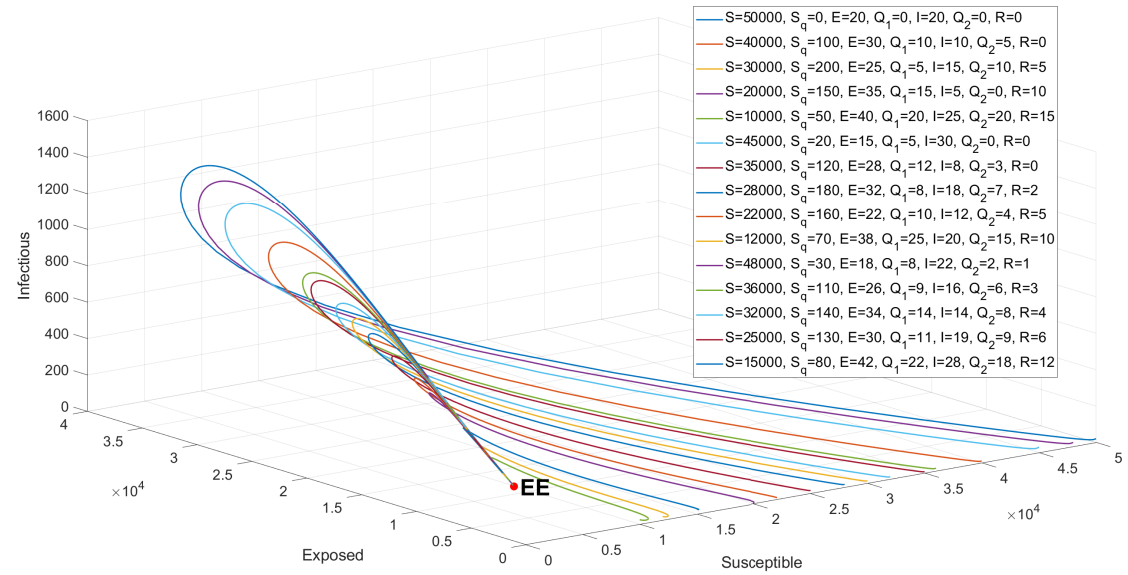

Figure 5. System trajectories under Condition 2 ($R_0 > 1$), converging to the EE.

Condition 4: Effect of self-protection. $\alpha = 0.85$, $\beta_1 = 0.00003$, $\beta_2 = 0.00003$, $\omega_2 = 0.01$, $\sigma_1 = 0.001$, $\sigma_2 = 0.001$, $\epsilon_1 = 0.2$, $\epsilon_2 = 0.2$, $\xi_1 = 0.038$, $\xi_2 = 0.01$, $\delta_1 = 0.5$, $\delta_2 = 0.5$, $\delta_3 = 0.5$, $\Lambda = 1$, $d = 0.0001$, $\alpha = 0.85$, $X(0) = (20000, 0, 20, 0, 20, 0, 0)$ and ω_1 have different values $(0.01, 0.04, 0.1, 0.2, 0.5)$.

Based on the parameter settings of **Condition 4**, Figure 6 shows the epidemiological dynamics of the seven compartments and the impact of the self-protection rate ω_1 on the basic reproduction number R_0 and each compartment. Figure 6h shows, according to Eq (3.3), that the self-protection rate ω_1 appears in the denominator term $d^\alpha + \omega_1^\alpha + \omega_2^\alpha$ of $R_0(\alpha)$. Consequently, as ω_1 increases, this denominator expands rapidly, causing R_0 to drop sharply; as ω_1 increases further, the sublinear growth of ω_1^α slows the denominator's increase, so the decline of R_0 also decelerates, indicating that enhanced self-protection measures can effectively reduce the risk of epidemic spread. In Figures 6a and 6b, the numbers of susceptible individuals S and self-protected susceptible individuals S_q decrease rapidly over time, and the higher the self-protection rate, the faster the reduction, demonstrating that self-protection measures significantly reduce the exposure of susceptible individuals to infection. For exposed individuals E and infected individuals I (Figures 6c and 6e), increasing the self-protection rate causes their numbers to decline rapidly, indicating that enhanced self-protection behaviors reduce the chances of exposure and infection, thus curbing further transmission of the epidemic.

Therefore, increasing the self-protection rate can effectively reduce the number of exposed and infected individuals, contributing to overall epidemic control. We recommend that policymakers and health authorities sustain robust public health campaigns to disseminate evidence-based protective measures through multiple channels; ensure adequate supply of personal protective equipment such as masks and disinfectants; and incorporate self-protection awareness into emergency response plans and routine control policies, so that in the event of future outbreaks, the public can be swiftly mobilized and the response effectively coordinated.

Condition 5: Effect of nucleic acid testing. $\alpha = 0.85$, $\beta_1 = 0.00003$, $\beta_2 = 0.00003$, $\omega_1 = 0.4$, $\omega_2 = 0.02$, $\epsilon_1 = 0.2$, $\epsilon_2 = 0.2$, $\xi_1 = 0.038$, $\xi_2 = 0.01$, $\delta_1 = 0.5$, $\delta_2 = 0.5$, $\delta_3 = 0.5$, $\Lambda = 1$, $d = 0.0001$, $\alpha = 0.85$, $X(0) = (20000, 0, 20, 0, 20, 0, 0)$ and σ_1 σ_2 have different values $(0.005, 0.01, 0.05, 0.1, 0.5)$.

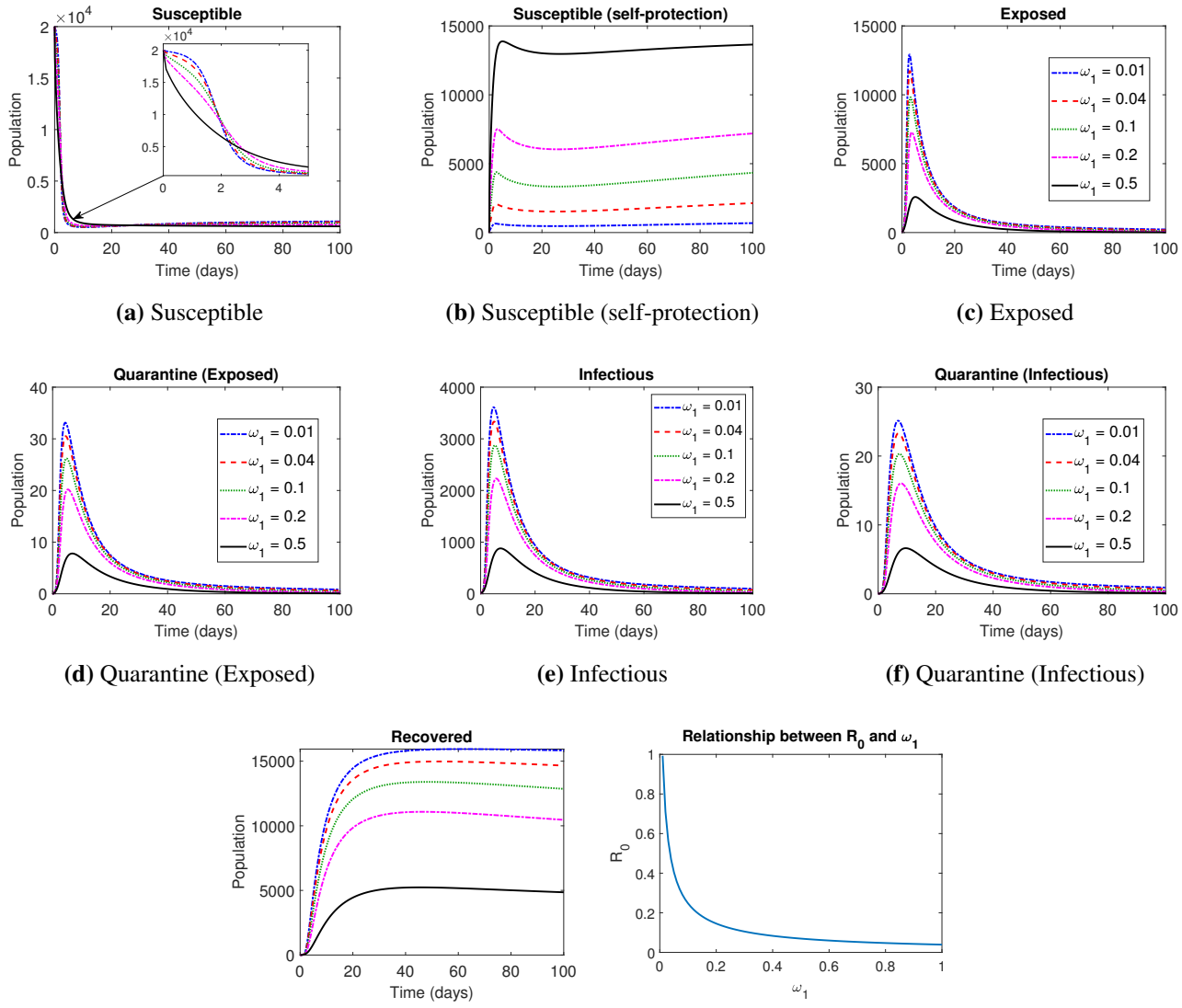

(a) Susceptible **(b)** Susceptible (self-protection) **(c)** Exposed

(d) Quarantine (Exposed) **(e)** Infectious **(f)** Quarantine (Infectious)

(g) Recovered **(h)** Relationship between R_0 and ω_1

Figure 6. Epidemiological dynamics of the seven compartments for different values of ω_1 and relationships between R_0 and ω_1. Here, $R_0 < 1$.

Based on the parameter settings of **Condition 5**, Figures 7h and 7i illustrate, based on Eq (3.3), how the proportion of positive tests σ_1 and σ_2 affect the basic reproduction number R_0: σ_1^α appears in the denominator factor $d^\alpha + \epsilon_1^\alpha + \sigma_1^\alpha$, while σ_2^α occurs both in the numerator term $\beta_1^\alpha \sigma_2^\alpha$ and in the denominator factor $d^\alpha + \delta_2^\alpha + \xi_1^\alpha + \sigma_2^\alpha$. As the proportion of positive tests increases, these denominator factors expand rapidly, significantly shortening the "residence time" of exposed and infectious individuals and causing R_0 to plummet; as test positivity continues to rise, the sublinear growth of σ_i^α slows this expansion, and the decline of R_0 correspondingly decelerates. As shown in Figure 7, the number of exposed individuals E and infected individuals I decreases significantly as testing increases, demonstrating that early identification and isolation measures reduce the transmission chain. Moreover, the numbers of quarantined exposed individuals Q_1 and quarantined infected individuals Q_2 increase as testing rates rise, indicating that stronger testing efforts lead to the rapid identification

and isolation of more exposed and infected individuals, significantly enhancing the effectiveness of quarantine measures and curbing the spread of the epidemic. Therefore, increasing nucleic acid testing can effectively reduce the number of exposed and infected individuals, enhance quarantine efficiency, and accelerate epidemic control. To this end, we recommend that government and health authorities expand testing capacity by establishing more fixed and mobile testing sites; streamline sampling and reporting processes to create a "early detection-early isolation-early treatment" closed loop; and incorporate testing metrics into emergency response plans and routine evaluations, ensuring rapid response and precise resource deployment in future outbreaks.

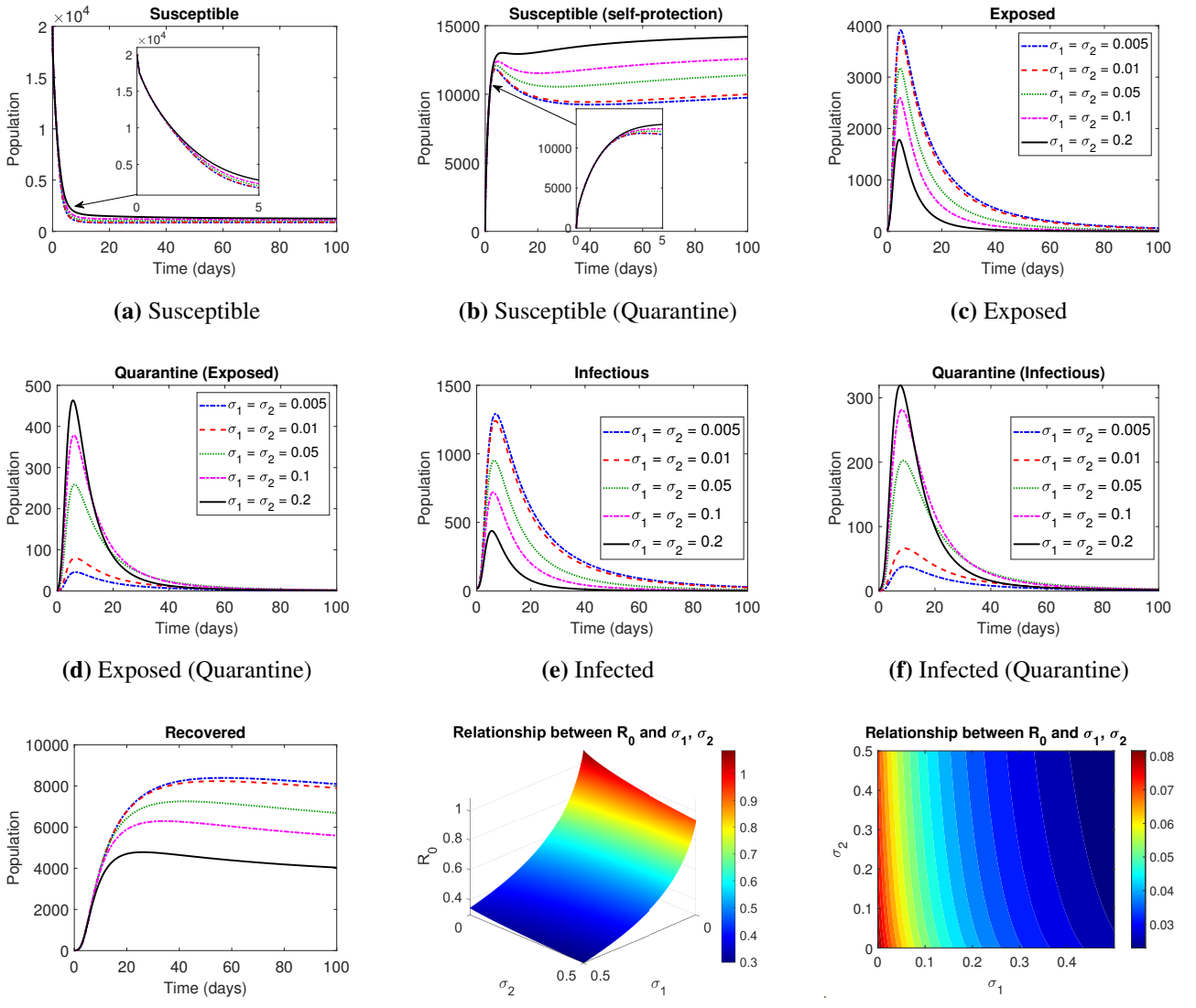

(a) Susceptible **(b)** Susceptible (Quarantine) **(c)** Exposed

(d) Exposed (Quarantine) **(e)** Infected **(f)** Infected (Quarantine)

(g) Recovered **(h)** Relationship between R_0 and σ_1, σ_2 (3D) **(i)** Relationship between R_0 and σ_1, σ_2 (Contour)

Figure 7. Epidemiological dynamics of the seven compartments for different values of σ_1 and σ_2, and the relationship between R_0 and σ_1, σ_2. Here, $R_0 < 1$.

5. Model fitting

In this section, we utilize COVID-19 data from Malaysia [51] to systematically estimate and calibrate model parameters, thereby validating the model's applicability and investigate the effects of nucleic acid testing and self-protection measures on transmission dynamics. First, a genetic algorithm is employed to obtain preliminary parameter values, which are then finely tuned via nonlinear least squares. The calibrated parameters are used to solve the model using the fractional-order forward Euler method [31] and generate fitting curves. We proceed with an error analysis, juxtaposing the fractional-order main model with its integer-order counterpart and a simplified fractional SEIR model, highlighting how the Caputo derivative's memory effect and the inclusion of self-protection, testing, and isolation mechanisms decisively enhance predictive accuracy. Finally, sensitivity and uncertainty analyses reveal the outstanding effectiveness of non-pharmaceutical interventions in controlling the COVID-19 outbreak in Malaysia. The detailed algorithmic workflow is outlined in Algorithm 1, encompassing the global search via GA, LSQ-based refinement, and the numerical solution using the fractional-order forward Euler scheme.

Algorithm 1 GA–LSQ fitting with the fractional forward Euler (FFE) scheme.

Require: Active–case series (Malaysia, 29 Sep–27 Nov 2020, N=60)

Ensure: $fittedParams$, I_{fitted}

1: **Pre-process:** $t_{\text{data}} \leftarrow$ days(29 Sep 2020 – 27 Nov 2020), $I_{\text{data}} \leftarrow$ active_cases [51]

2: **Bounds:** specify lower and upper bounds for each of the 16 parameters (see Table 3).

3: **Objective** obj(par):

$I_{\text{fitted}} \leftarrow \text{FFE}(par, t_{\text{data}})$

if I_{fitted} has NaN/Inf **then** obj(par) = ∞

else obj(par) = $\sum (I_{\text{data}} - I_{\text{fitted}})^2$

4: **GA phase (200 pop., 1000 gen.):**

`GA_opts = optimset('ga', 'PopulationSize', 200, 'MaxGenerations', 1000)`

$par^{(0)} \leftarrow$ `ga`(obj, 16, lb, ub, GA_opts); clip to [lb, ub]

5: **LSQ refinement:**

`LSQ_opts = optimset('TolX',1e-12,'TolFun',1e-12,'MaxFunEvals',5000)`

try

$fittedParams \leftarrow$ `lsqcurvefit`(FFE, $par^{(0)}$, t_{data}, I_{data}, lb, ub, LSQ_opts)

catch $fittedParams \leftarrow par^{(0)}$

6: **Fit via FFE:** $I_{\text{fitted}} \leftarrow \text{FFE}(fittedParams, t_{\text{data}})$

7: **FFE core update for compartment** $X \in \{S, S_q, E, I, Q_1, Q_2, R\}$**:**

$$X_j = X_{j-1} + \frac{h_j^\alpha}{\Gamma(1+\alpha)} \sum_{k=1}^{j-1} \left[(j-k+1)^\alpha - (j-k)^\alpha \right] f_X(t_k, X_k).$$

8: **return** $fittedParams$, I_{fitted}

To obtain initial estimates of model parameters, we employ a genetic algorithm to search the

following parameter ranges: $\alpha, \beta_1, \beta_2, \omega_1, \omega_2, \sigma_1, \sigma_2, \epsilon_1, \epsilon_2, \lambda_1, \lambda_2, \delta_1, \delta_2, \delta_3, \Lambda$, and d. The initial state of the population is set as $X(0) = (3557000, 0, 1061, 0, 1061, 0, 0)$. After completing the parameter search and estimation, the estimated parameters, their search ranges, and the corresponding 95% confidence intervals are summarized in Table 3, and the final fitting results are shown in Figure 8.

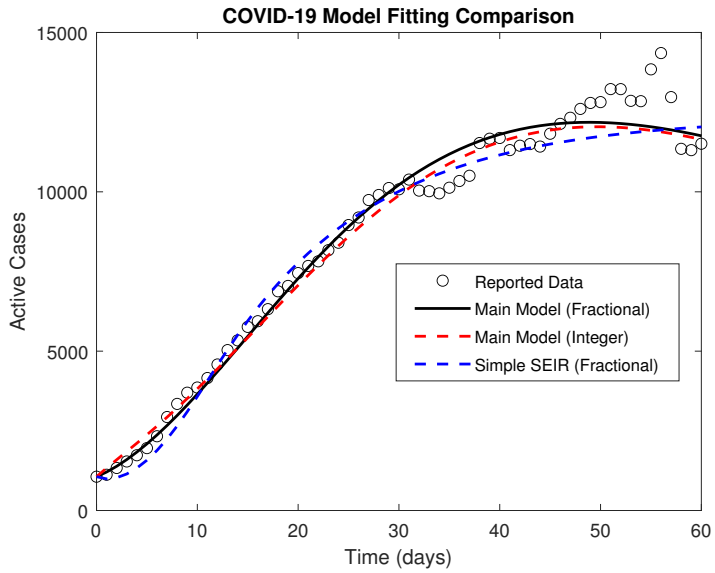

Figure 8. Comparison of integer-order, major fractional-order models and simplified SEIR fractional model in fitting COVID-19 active cases in Malaysia (Date: 29.09.2020-27.11.2020) (60 days).

Table 3. Parameter estimation for Malaysia: Point estimates, search bounds, and 95% confidence intervals.

Parameter	Estimate	Lower bound	Upper bound	95% CI
α	0.9004	0.5	1.0	$[0.8999, 0.9010]$
β_1	9.9752×10^{-10}	1×10^{-10}	1×10^{-5}	$[9.9465,\ 9.9896] \times 10^{-10}$
β_2	9.7882×10^{-10}	1×10^{-10}	1×10^{-5}	$[9.7582,\ 9.7975] \times 10^{-10}$
ω_1	0.0456	0.01	0.5	$[0.0431, 0.0473]$
ω_2	0.0098	0.001	0.5	$[0.0095, 0.0102]$
σ_1	0.0154	0.001	0.5	$[0.0126, 0.0189]$
σ_2	0.0197	0.001	0.5	$[0.0185, 0.0216]$
ϵ_1	0.2096	0.1	0.5	$[0.1934, 0.2166]$
ϵ_2	0.1024	0.1	0.5	$[0.0947, 0.1179]$
ξ_1	0.0296	0.001	0.05	$[0.0284, 0.0315]$
ξ_2	0.0103	0.001	0.05	$[0.0096, 0.0114]$
δ_1	0.0027	0.0001	0.1	$[0.0024, 0.0031]$
δ_2	0.0138	0.0001	0.1	$[0.0125, 0.0157]$
δ_3	0.0041	0.0001	0.1	$[0.0034, 0.0047]$
Λ	0.9820	0	1000.0	$[0.9718, 0.9921]$
d	1.45×10^{-5}	1.1×10^{-5}	3.2×10^{-5}	$[1.4179,\ 1.4766] \times 10^{-5}$

Figure 8 presents the evolution of active COVID-19 cases in Malaysia and the fitting performance of three models. The solid black curve (fractional order main model) closely traces the scattered data points throughout the rising and falling phases, demonstrating superior accuracy. The red dashed curve (integer-order main model) slightly deviates from the actual case numbers during the early growth and peak periods, indicating that a integer-order approach lacks sufficient memory effects. The blue dashed curve (simplified fractional SEIR model [52]) fits the initial trend reasonably well but deviates significantly in the middle and later stages, reflecting the limitations of its reduced compartmental structure. It is clear that the superior performance of the main fractional order model stems from its more complex framework, which incorporates public self protection awareness as well as nucleic acid testing and isolation measures. This comprehensive approach better matches the actual epidemic conditions in Malaysia and provides a more reliable basis for evaluating intervention strategies.

To quantitatively assess the predictive accuracy of the main integer-order (ODE) model, the main fractional-order (FODE) model, and the simplified fractional SEIR (F-SEIR) model, we employ the following error metrics: Root mean square error (RMSE), mean absolute error (MAE), and mean absolute percentage error (MAPE).

$$\text{RMSE} = \sqrt{\frac{1}{n}\sum_{i=1}^{n}(y_i - \hat{y}_i)^2}, \tag{5.1}$$

$$\text{MAE} = \frac{1}{n}\sum_{i=1}^{n}|y_i - \hat{y}_i|, \tag{5.2}$$

$$\text{MAPE} = \frac{100\%}{n}\sum_{i=1}^{n}\left|\frac{y_i - \hat{y}_i}{y_i}\right|. \tag{5.3}$$

Here, y_i is the observed data, $\hat{y}_i$ is the model prediction, and n is the total number of observations.

In Table 4, we compare the main integer order model, the main fractional order model, and the simplified SEIR fractional model over days 1 to 20, days 21 to 40, days 41 to 60 and overall days 1 to 60 in terms of RMSE, MAE, and MAPE. The main FODE model achieves the lowest errors in both the early stage and the overall period, demonstrating its memory term's precise capture of exponential growth and tail decay. During days 21 to 40, the main ODE model shows a slightly lower RMSE (439.92 versus 518.33), which is consistent with the local fluctuations seen in Figure 8, suggesting that the fractional-order memory may continue to be influenced by the early epidemic dynamics. The simplified SEIR model exhibits substantially higher errors at all stages, reflecting its oversimplified structure's inability to capture late-stage complex dynamics. These findings confirm that the main fractional order model, by integrating memory effects together with self-protection awareness, testing and isolation measures, outperforms the other two models and provides the most accurate fit across the epidemic cycle.

Table 4. Comparison of the main ODE model, FODE main model, and F-SEIR model fitting errors.

	ODE main model			FODE main model			Simple F-SEIR		
Time Period	**RMSE**	**MAE**	**MAPE (%)**	**RMSE**	**MAE**	**MAPE (%)**	**RMSE**	**MAE**	**MAPE (%)**
Days 1–20	272.77	241.76	8.3825	219.58	191.80	5.1639	382.35	330.91	11.299
Days 21–40	439.92	381.20	3.8675	518.33	350.46	3.5088	407.08	371.50	3.8153
Days 41–60	947.87	736.93	5.6892	889.83	721.56	5.6463	1048.40	856.56	6.6369
Overall (1–60)	623.54	453.30	5.9797	607.92	421.27	4.7730	685.84	519.66	7.2505

Figure 9a illustrates the sensitivity of active-case trajectories to the protective-awareness parameter ω_1: As ω_1 increases from 0.040 to 0.100, the epidemic peak height decreases progressively, and the peak timing advances, with the highest awareness scenario (purple) reducing the peak to less than half the baseline (blue). Figure 9c compares combined testing rates σ_1 and σ_2 at 0.005, 0.010, 0.020, and 0.050: Higher testing levels shift the peak downward and earlier, and at 0.050, the curve plateaus by day 40 before declining sharply, confirming the effectiveness of early "test-isolate" interventions. Figures 9b and 9d overlay the 95% confidence intervals (pink shading) derived from sampling ω_1 and σ_1, σ_2: Both the median trajectory (red) and the best-fit curve (blue) remain comfortably within these bands, demonstrating the model's internal consistency and robustness over the mid-term. Notably, the confidence bands widen markedly toward the end of the 60-day horizon, indicating that small parameter perturbations accumulate to reduce long-term predictive certainty.

In conclusion, we recommend sustained public education through multiple channels to reinforce mask-wearing, hand hygiene, and social distancing; a substantial expansion of testing capacity and accessibility by deploying mobile units and streamlining sample collection for early detection and isolation; and, in particular, intensified screening in high-risk areas combined with data-driven, targeted interventions based on historical trends. These measures will further suppress viral spread and safeguard public health.

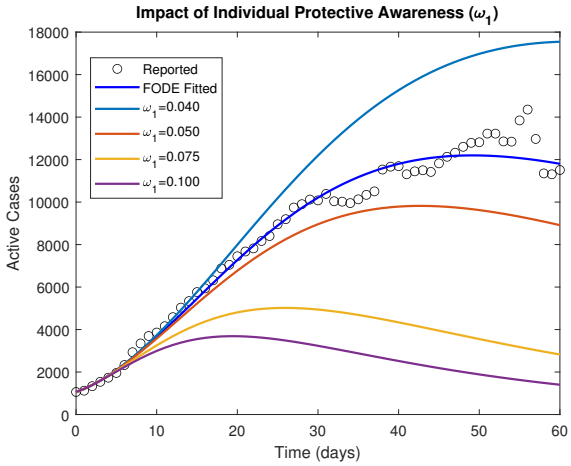

(a) Impact of individual protective awareness ω_1

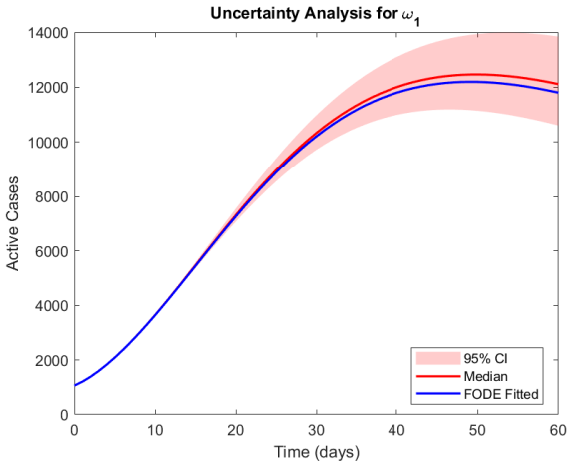

(b) Uncertainty analysis for individual protective awareness ω_1

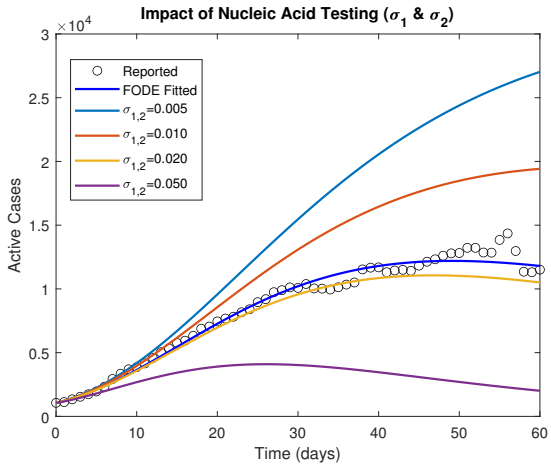

(c) Impact of nucleic acid testing σ_1 & σ_2

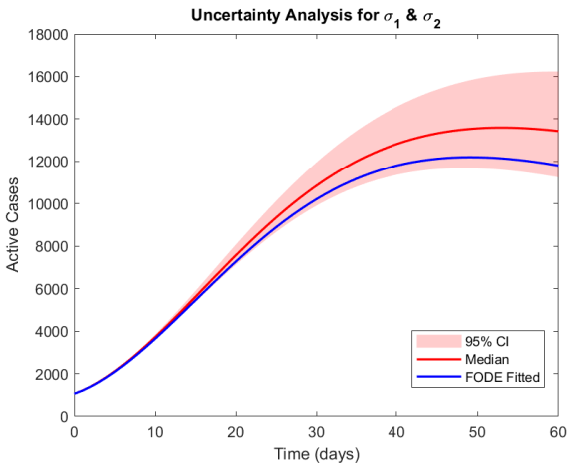

(d) Uncertainty analysis for testing σ_1 & σ_2

Figure 9. Sensitivity and uncertainty analysis of individual protective awareness and testing.

6. Fractional optimal control of the model

To translate our modeling results into practical epidemic control measures, we recast the Caputo fractional order COVID19 dynamic model as an optimal control problem constrained by Malaysia's current healthcare resources and capacity limits, with the goal of minimizing total societal cost. We introduce two key control variables: Personal protective awareness and nucleic acid testing intensity. Using the Pontryagin's Maximum Principle [53], we derive optimal interventions and develop six representative strategies. The cost function captures the health economic burden of each compartment and the cost of implementing the corresponding measures, ensuring that the model outputs quantify cost benefit and reflect real world feasibility. We then examine how careful tuning of these controls can effectively curb disease transmission and provide decision makers with a rigorous and actionable framework in detail.

6.1. Description of optimal control function

We reconstruct a fractional-order model with optimal control based on model (2.1). The control variables u_1, u_2, and u_3 represent adjustments to the intensity of self-protection awareness and nucleic acid testing. It is important to note that these control variables are derived from the optimized substitution of the original model parameters ω_1, σ_1, and σ_2, as detailed as:

$$\begin{cases} {}^{C}D^{\alpha}S = \Lambda^{\alpha} + \omega_2^{\alpha}S_q - \beta_1^{\alpha}SE - \beta_2^{\alpha}SI - (u_1(t) + d^{\alpha})S, \\ {}^{C}D^{\alpha}S_q = u_1(t)S - (\omega_2^{\alpha} + d^{\alpha})S_q, \\ {}^{C}D^{\alpha}E = \beta_1^{\alpha}SE + \beta_2^{\alpha}SI - (\epsilon_1^{\alpha} + u_2(t) + d^{\alpha})E, \\ {}^{C}D^{\alpha}Q_1 = u_2(t)E - (\epsilon_2^{\alpha} + \delta_1^{\alpha} + d^{\alpha})Q_1, \\ {}^{C}D^{\alpha}I = \epsilon_1^{\alpha}E - (u_3(t) + \delta_2^{\alpha} + \xi_1^{\alpha} + d^{\alpha})I, \\ {}^{C}D^{\alpha}Q_2 = \epsilon_2^{\alpha}Q_1 + u_3(t)I - (\delta_3^{\alpha} + \xi_2^{\alpha} + d^{\alpha})Q_2, \\ {}^{C}D^{\alpha}R = \delta_1^{\alpha}Q_1 + \delta_2^{\alpha}I + \delta_3^{\alpha}Q_2 - d^{\alpha}R. \end{cases} \tag{6.1}$$

In order to balance reducing active infections with the economic costs of intervention, we introduce the following objective function:

$$J(u_1, u_2, u_3) = \int_{t_0}^{t_r} L(E, Q_1, I, Q_2, u_1, u_2, u_3)dt, \tag{6.2}$$

where

$$L(E, Q_1, I, Q_2, u_1, u_2, u_3) = B_0E(t) + B_1Q_1(t) + B_2I(t) + B_3Q_2(t) + B_4u_1^2(t) + B_5u_2^2(t) + B_6u_3^2(t). \tag{6.3}$$

In our optimal-control framework, the instantaneous cost consists of two parts: (i) The socio-economic burden of individuals in compartments E, Q_1, I, and Q_2, characterized by the dimensionless weights B_0, B_1, B_2, and B_3, each normalized to the daily cost of one uncontrolled infection and portraying their socio-economic impact, including healthcare resource allocation and management costs; and (ii) the resource expenditure of interventions, quantified by B_4, B_5, and B_6 as the costs of protective awareness campaigns and nucleic acid testing efforts. This unified scaling ensures that healthcare utilization and intervention spending are measured on the same scale and align with Malaysia's real-world capacity and budget constraints.

The Hamiltonian function $H(S, S_q, E, Q_1, I, Q_2, R, u_j, \pi_i)$ is defined as

$$H = L(I, u_1, u_2, u_3) + \sum_{i=1}^{7} \pi_i f_i, \tag{6.4}$$

where $\pi_i (i = 1, 2, 3, 4, 5, 6, 7)$ are the adjoint variables, and f_i are the constraint functions in the context of Lagrange multipliers obtained from model (6.1).

From the Hamiltonian function (6.4), we have

$$\begin{aligned} H(S, S_q, E, Q_1, I, Q_2, R, u_j, \pi_i) = {} & B_0E(t) + B_1Q_1(t) + B_2I(t) + B_3Q_2(t) + B_4u_1^2(t) + B_5u_2^2(t) + B_6u_3^2(t) \\ & + \pi_1\left[\Lambda^\alpha + \omega_2^\alpha S_q(t) - \beta_1^\alpha S(t)E(t) - \beta_2^\alpha S(t)I(t) - (u_1(t) + d^\alpha)S(t)\right] \\ & + \pi_2\left(u_1(t)S(t) - (\omega_2^\alpha + d^\alpha)S_q(t)\right) \\ & + \pi_3\left[\beta_1^\alpha S(t)E(t) + \beta_2^\alpha S(t)I(t) - (\epsilon_1^\alpha + u_2(t) + d^\alpha)E(t)\right] \\ & + \pi_4\left[u_2(t)E(t) - (\epsilon_2^\alpha + \delta_1^\alpha + d^\alpha)Q_1(t)\right] \\ & + \pi_5\left(\epsilon_1^\alpha E(t) - (u_3(t) + \delta_2^\alpha + \xi_1^\alpha + d^\alpha)I(t)\right) \\ & + \pi_6\left[\epsilon_2^\alpha Q_1(t) + u_3(t)I(t) - (\delta_3^\alpha + \xi_2^\alpha + d^\alpha)Q_2(t)\right] \\ & + \pi_7\left[\delta_1^\alpha Q_1(t) + \delta_2^\alpha I(t) + \delta_3^\alpha Q_2(t) - d^\alpha R(t)\right]. \end{aligned} \tag{6.5}$$

According to Pontryagin's Maximum Principle, we have

$$\begin{aligned} {}^CD^\alpha\pi_1 &= -\frac{\partial H}{\partial S} = \pi_1\beta_1^\alpha E(t) + \pi_1\beta_2^\alpha I(t) + \pi_1(u_1(t) + d^\alpha) - \pi_2u_1(t) - \pi_3\beta_1^\alpha E(t) - \pi_3\beta_2^\alpha I(t), \\ {}^CD^\alpha\pi_2 &= -\frac{\partial H}{\partial S_q} = -\pi_1\omega_2^\alpha + \pi_2(\omega_2^\alpha + d^\alpha), \\ {}^CD^\alpha\pi_3 &= -\frac{\partial H}{\partial E} = -B_0 + \pi_1\beta_1^\alpha S(t) - \pi_3\beta_1^\alpha S(t) + \pi_3(\epsilon_1^\alpha + u_2(t) + d^\alpha) - \pi_4u_2(t) - \pi_5\epsilon_1^\alpha, \\ {}^CD^\alpha\pi_4 &= -\frac{\partial H}{\partial Q_1} = -B_1 + \pi_4(\epsilon_2^\alpha + \delta_1^\alpha + d^\alpha) - \pi_6\epsilon_2^\alpha - \pi_7\delta_1^\alpha, \\ {}^CD^\alpha\pi_5 &= -\frac{\partial H}{\partial I} = -B_2 + \pi_1\beta_2^\alpha S(t) - \pi_3\beta_2^\alpha S(t) + \pi_5(u_3(t) + \delta_2^\alpha + \xi_1^\alpha + d^\alpha) - \pi_6u_3(t) - \pi_7\delta_2^\alpha, \\ {}^CD^\alpha\pi_6 &= -\frac{\partial H}{\partial Q_2} = -B_3 + \pi_6(\delta_3^\alpha + \xi_2^\alpha + d^\alpha) - \pi_7\delta_3^\alpha, \\ {}^CD^\alpha\pi_7 &= -\frac{\partial H}{\partial R} = \pi_7d^\alpha. \end{aligned}$$

The transversality conditions at the terminal time t_r are

$$\pi_1(t_r) = \pi_2(t_r) = \pi_3(t_r) = \pi_4(t_r) = \pi_5(t_r) = \pi_6(t_r) = \pi_7(t_r) = 0.$$

Theorem 8. *To minimize $J^*(u_1^*, u_2^*, u_3^*) = \min_{(u_1,u_2,u_3)\in U} J(u_1, u_2, u_3)$, the optimal control strategies are determined as follows:*

$$u_1^* = \min\left\{\max\{u_1^{\min}, \tfrac{(\pi_1-\pi_2)S(t)}{2B_4}\}, u_1^{\max}\right\},$$

$$u_2^* = \min\left\{\max\{u_2^{\min}, \tfrac{(\pi_3-\pi_4)E(t)}{2B_5}\}, u_2^{\max}\right\},$$

$$u_3^* = \min\left\{\max\{u_3^{\min}, \tfrac{(\pi_5-\pi_6)I(t)}{2B_6}\}, u_3^{\max}\right\}.$$

Proof of Theorem 8. According to the control conditions, the Hamiltonian function can be obtained:

$$\frac{\partial H}{\partial u_1} = 2B_4\, u_1^* - \pi_1\, u_1^* S(t) + \pi_2\, u_1^* S(t) = 0,$$
$$\frac{\partial H}{\partial u_2} = 2B_5\, u_2^* - \pi_3\, u_2^* E(t) + \pi_4\, u_2^* E(t) = 0,$$
$$\frac{\partial H}{\partial u_3} = 2B_6\, u_3^* - \pi_5\, u_3^* I(t) + \pi_6\, u_3^* I(t) = 0.$$

Then, we get

$$u_1^* = \frac{(\pi_1 - \pi_2)S(t)}{2B_4}, \quad u_2^* = \frac{(\pi_3 - \pi_4)E(t)}{2B_5}, \quad u_3^* = \frac{(\pi_5 - \pi_6)I(t)}{2B_6}.$$

Conditions for determining u_1^*, u_2^*, and u_3^*:

$$u_1^* = \begin{cases} u_1^{min}, & \text{if } \frac{\partial H}{\partial u_1} < 0, \\ 0 < \frac{(\pi_1-\pi_2)S(t)}{2B_4} < 1, & \text{if } \frac{\partial H}{\partial u_1} = 0, \\ u_1^{max}, & \text{if } \frac{\partial H}{\partial u_1} > 0. \end{cases}$$

$$u_2^* = \begin{cases} u_2^{min}, & \text{if } \frac{\partial H}{\partial u_2} < 0, \\ 0 < \frac{(\pi_3-\pi_4)E(t)}{2B_5} < 1, & \text{if } \frac{\partial H}{\partial u_2} = 0, \\ u_2^{max}, & \text{if } \frac{\partial H}{\partial u_2} > 0. \end{cases}$$

$$u_3^* = \begin{cases} u_3^{min}, & \text{if } \frac{\partial H}{\partial u_3} < 0, \\ 0 < \frac{(\pi_5-\pi_6)I(t)}{2B_6} < 1, & \text{if } \frac{\partial H}{\partial u_3} = 0, \\ u_3^{max}, & \text{if } \frac{\partial H}{\partial u_3} > 0. \end{cases}$$

Thus, for each time t, the optimal control $u_i^*(t)(i = 1, 2, 3)$ is determined by whether the partial derivative $\frac{\partial H}{\partial u_i}$ is positive, negative, or zero. By substituting these optimal controls back into the dynamic equations and the cost functional, one can verify that they minimize the Hamiltonian at every moment, thereby satisfying the necessary conditions for optimality. □

6.2. Numerical results of the optimal control

Leveraging the Pontryagin's Maximum Principle together with a forward-backward PECE algorithm [31], we derive time-varying optimal control strategies that minimize cumulative societal cost under realistic resource and capacity constraints. We validate these strategies by comparing simulated epidemic trajectories against actual COVID-19 data from Malaysia. Each strategy is then evaluated based on cumulative cost and average cost-effectiveness ratio (ACER) [54] to highlight its relative merits and implementability. Six primary intervention strategies are examined:

- **Strategy 1:** Joint optimization of protective awareness campaigns and nucleic acid testing coverage;
- **Strategy 2:** Adjustment of protective awareness campaigns alone, while maintaining baseline testing levels;

- **Strategy 3:** Sole modulation of testing coverage, while maintaining baseline protective awareness levels;
- **Strategies 4–6:** Enhanced protective awareness campaigns with testing coverage caps set at 0.1, 0.3, and 0.5 respectively.

All model parameters, except for the control variables, are taken directly from Table 3, and the epidemic is initialized with $X(0) = (3557000, 0, 1061, 0, 1061, 0, 0)$ To compute the time-dependent optimal controls, we employ Algorithm 2: The forward-backward PECE scheme for optimal control, which alternates between forward integration of the state equations and backward integration of the adjoint system until convergence criteria are met.

We reference the Malaysian Ministry of Health report [55] and adopt a baseline treatment cost of RM 870 per day for a critically ill COVID-19 patient to calibrate the dimensionless cost weights B_0–B_3. Concretely, we set $B_2 = 1.0$ (RM 870/day, active unisolated infections), $B_0 = 0.8$ (RM 696/day, exposed individuals in the community), $B_3 = 0.5$ (RM 435/day, infectious cases under quarantine), and $B_1 = 0.4$ (RM 348/day, quarantined exposed persons). This ordering captures the greater societal burden posed by undiagnosed individuals, who incur higher transmission risk and productivity losses, while reflecting the reduced impact of quarantined groups. Mapping these coefficients to Malaysian Ringgit ensures that our model's cost estimates are directly comparable to real healthcare expenditures and policy budgets.

In order to quantify the resource requirements of our interventions, we assign the cost weight $B_4 = 0.01$ to protective awareness campaigns and $B_5 = B_6 = 0.05$ to testing activities. Using a reference cost of RM 870 per day for an uncontrolled infection, these weights correspond to approximately RM 8.7 per person per day for awareness campaigns, reflecting average monthly media and community outreach expenses and RM 43.5 per person per day for testing covering staffing reagents and logistics. Strategies 1 to 3 assume full implementation with $u_1^{\max} = u_2^{\max} = u_3^{\max} = 1$. Strategies 4 to 6 impose testing capacity limits by setting $u_2^{\max}$ and $u_3^{\max}$ to 0.1, 0.3, and 0.5, respectively, to emulate laboratory throughput constraints in Malaysia while maintaining $u_1^{\max} = 1$ to ensure sustained outreach effort. Table 5 and Figure 10 show each strategy's costs and active case outcomes.

Table 5. Cumulative cost and ACER for different strategies.

Strategy	Cumulative Cost	ACER
Strategy 1	46118.4	0.0748
Strategy 2	61690.6	0.1067
Strategy 3	53347.0	0.0865
Strategy 4	55715.7	0.0930
Strategy 5	50636.4	0.0828
Strategy 6	48556.1	0.0790
Malaysia	883273.0	–

Algorithm 2 Forward-Backward PECE scheme with three controls $u_{1,2,3}$.

Require: N, α, parameters $\{p_i\}$, initial states $X(0)$, weights $k_{1,2,3}$, projection proj$(\cdot)$, tolerance ε
Ensure: Optimal states $X(t) = \{S, S_q, E, I, Q_1, Q_2, R\}$, adjoints $\pi_i(t)(i = 1, 2, \ldots, 7)$, controls $\mathbf{u}^*(t)$

Initialise states $(S, S_q, E, Q_1, I, Q_2, R)$ and controls $u_{1,2,3} \leftarrow 0$
repeat
  for $j = 1$ **to** $N - 1$ **do**
    compute fractional weights $b_m = m^\alpha - (m-1)^\alpha$, $a_m = (m+1)^{\alpha+1} - 2m^{\alpha+1} + (m-1)^{\alpha+1}$
    Predict $(X \in \{S, S_q, E, Q_1, I, Q_2, R\})$

$$X_j^P = X_{j-1} + \frac{h^\alpha}{\Gamma(1+\alpha)} \sum_{k=1}^{j-1} b_{\,j-k+1}\, f_X(t_k, X_k, u_k), \tag{P1}$$

    Correct

$$X_j = X_{j-1} + \frac{h^\alpha}{\Gamma(2+\alpha)}\Big[f_X(t_j, X_j^P, u_j) + f_X(t_0, X_0, u_0) + \sum_{k=1}^{j-1} a_{\,j-k}\, f_X(t_k, X_k, u_k)\Big], \tag{C1}$$

  end for
  reverse state arrays; set $\pi_i(t_{\text{final}}) = 0$
  for $j = 1$ **to** $N - 1$ **do**
    Predict $(\pi_i,\ i = 1 \ldots 7)$

$$\pi_{i,j}^P = \frac{h^\alpha}{\Gamma(1+\alpha)} \sum_{k=1}^{j-1} b_{\,j-k+1}\, g_i(t_k, X_k, \pi_k, u_k), \tag{P2}$$

    Correct

$$\pi_{i,j} = \frac{h^\alpha}{\Gamma(2+\alpha)}\Big[g_i(t_j, X_j, \pi_j^P, u_j) + g_i(t_0, X_0, \pi_0, u_0) + \sum_{k=1}^{j-1} a_{\,j-k}\, g_i(t_k, X_k, \pi_k, u_k)\Big], \tag{C2}$$

  end for
  update controls (projected PMP):

$$u_1 \leftarrow \text{proj}((\pi_1 - \pi_2)S/(2k_1)),$$
$$u_2 \leftarrow \text{proj}((\pi_3 - \pi_4)E/(2k_2)),$$
$$u_3 \leftarrow \text{proj}((\pi_5 - \pi_6)I/(2k_3)),$$

  then relax $u_i \leftarrow (u_i^{\text{new}} + u_i^{\text{old}})/2$
  $\Delta = \max_{i=1,2,3}\left|u_i^{\text{new}} - u_i^{\text{old}}\right|$.
  $u^{\text{old}} \leftarrow u^{\text{new}}$
until $\Delta < \varepsilon$
return $X(t), \pi_i(t), \mathbf{u}^*(t)$

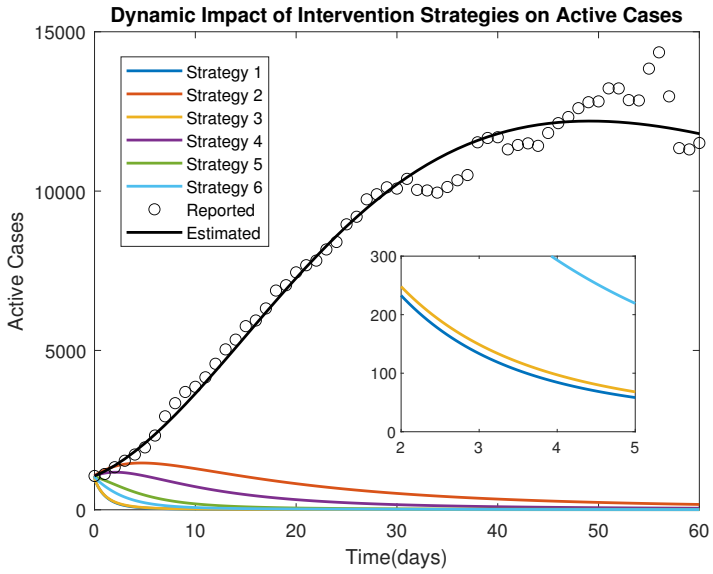

Figure 10. Comparison of reported active COVID-19 cases in Malaysia, fitted, and model-based estimates under six control strategies.

Figure 10 compares reported active cases, the fitted curve, and model predictions for six intervention strategies to show their dynamic effects. Strategy 1 pairs strong awareness campaigns with wide testing and achieves the lowest peak, the fastest case decline, the fewest total cases, the lowest overall cost, and the best cost effectiveness ratio. Strategy 2 uses awareness only, which reduces spread somewhat, but without testing, the peak is higher and the decline is slower. Strategy 3 uses testing only, which cuts the peak and cost per case more than Strategy 2, but only, which falls short of the combined approach. Strategies 4 to 6 model lab limits by capping testing intensity at 10%, 30%, and 50% while keeping awareness unchanged. Their curves lie between those of Strategies 1 and 2 and move closer to Strategy 1 as testing intensity rises. Notably, at a 30% cap, most benefits of full testing are gained at less than half the extra cost, showing that under Malaysia's real resource limits, medium testing plus strong awareness can give near optimal control.

Table 5 compares the cumulative cost and average cost-effectiveness ratio (ACER) of each strategy against the real-world scenario cost of 883273.0 model units. Strategy 1, which combines strong awareness campaigns with maximum testing intensity, reduces the cost to 46118.4 (a 94.8% reduction) and achieves the lowest ACER (0.0748), setting the optimal benchmark. In contrast, Strategy 2 (awareness only) incurs the highest cost (61690.6) and the worst ACER (0.1067), indicating that awareness alone is insufficient to effectively control the epidemic. Strategy 3 (testing only) improves upon Strategy 2 in both cost (53347.0) and ACER (0.0865), yet falls short of the combined intervention. Strategies 4 through 6 maintain strong awareness while capping testing intensity at 10%, 30%, and 50%, respectively, resulting in incremental improvements: Strategy 4 costs 55715.7 with ACER 0.0930; Strategy 5 costs 50636.4 with ACER 0.0828; and Strategy 6 costs 48,556.1 with ACER 0.0790. Notably, Strategy 5 employs only 30% testing intensity yet achieves over 85% of the cost and ACER improvements of Strategy 1, with its ACER only about 10.7% higher than the optimal. This demonstrates that under resource constraints, combining 30% testing intensity with strong awareness yields a relatively cost-effective epidemic control outcome, representing the best balance between

effectiveness and feasibility for public health policymaking.

Under Malaysia's current public health infrastructure and fiscal resources, a combined approach of strong awareness campaigns and a moderate testing intensity is both feasible and highly cost-effective. Leveraging the MySejahtera app and over 700 public testing laboratories enables us to maintain a moderate detection level within existing capacity without new construction, thereby conserving reagents and personnel. From a cost-effectiveness and operational standpoint, Strategy 5 delivers an incremental cost–effectiveness ratio of only 0.0828 model units (approximately RM 72 per case averted), far below the average hospitalization cost. Early detection and isolation sharply reduce downstream healthcare expenses, minimize workforce disruptions, and can prevent 0.1–0.2% of monthly GDP losses. Community clinics and mobile testing units can be deployed in a grid pattern to meet daily moderate detection targets while maintaining high-frequency outreach. This not only lowers the epidemic peak but also redirects saved resources toward vaccine rollout and treatment capacity. Even if testing costs rise or compliance falls, the combined strategy outperforms single measures. We recommend that health authorities set daily testing targets at a moderate detection level and sustain multi-channel awareness campaigns via TV, social media, and community mobilization to maximize budget efficiency, reduce peak caseloads, and mitigate economic and health impacts.

7. Discussion and conclusions

In this paper, we develop and rigorously analyze a Caputo fractional-order COVID-19 model that integrates nucleic acid testing and individual protective awareness to capture memory effects and the real-world impact of non-pharmaceutical interventions. Theoretical proofs establish the existence, non-negativity, and boundedness of solutions, and the next-generation matrix approach yields the basic reproduction number R_0. When $R_0 < 1$, the DFE is globally asymptotically stable; whereas when $R_0 > 1$, we establish conditions under which the EE is globally asymptotically stable. Numerical simulations using the ABM-PECE algorithm confirm the analytical findings. Furthermore, these simulations show that increasing public awareness or testing intensity can substantially reduce R_0, thereby effectively suppressing disease transmission across scenarios.

Subsequently, we employ a hybrid parameter estimation approach combining genetic algorithms and least-squares fitting, and use a fractional-order forward Euler algorithm for numerical simulation and model calibration against Malaysia's actual epidemic data. The fractional-order model demonstrates a superior fit compared to its integer-order counterpart and a simplified fractional-order SEIR model, highlighting the critical role of memory effects in epidemic forecasting. Moreover, by incorporating public protective awareness, nucleic-acid testing, and isolation measures, the model more accurately reflects Malaysia's real-world control practices. Sensitivity and uncertainty analyses further indicate that enhancing awareness campaigns or increasing testing intensity can significantly reduce the infection peak and total case count, providing a robust basis for designing more effective intervention strategies.

In our optimal-control analysis, six intervention strategies are designed using the Pontryagin's Maximum Principle and a forward-backward PECE algorithm, and each is assessed by cumulative cost and ACER. The combined "intensive awareness plus maximal testing" approach achieves the lowest total cost and the best ACER of all strategies. Moreover, while single interventions of awareness or testing can somewhat slow transmission, they struggle to balance cost and impact; the joint strategy,

however, offers clear advantages in reducing case numbers and managing expenses. Under laboratory capacity constraints, the mixed "strong awareness plus moderate testing" approach uses roughly half the testing resources while having an ACER only about 10.7% higher than the optimum, making it especially suitable when testing costs rise or compliance falls. Moreover, this strategy effectively keeps active community case counts low, providing a high-value solution for public health management.

Although we develope a Caputo fractional-order COVID-19 transmission model based on Malaysian outbreak data, integrating nucleic acid testing and individual protective awareness to capture memory effects and intervention impacts, the model remains limited to a short-term, single-wave scenario and operates under assumptions of constant parameters, homogeneous mixing, perfect testing, and instantaneous isolation. It does not incorporate multi-wave dynamics, time-varying parameters, or imperfect testing and isolation. In the future, we will focus on long-term, multi-wave epidemic contexts. First, time-varying transmission parameters will be introduced to dynamically reflect the effects of public health policies, behavioral changes, and viral evolution. Next, models of imperfect testing and isolation processes will be developed to account for test sensitivity and specificity, delays, and isolation failure rates. Finally, stochastic perturbations will be embedded within the fractional-order framework to simulate more realistic epidemic fluctuations and uncertainties.

Author contributions

Rui Hu: Writing – original draft, data curation, software, visualization, validation, methodology, conceptualization; Elayaraja Aruchunan: Writing – review & editing, validation, supervision; Muhamad Hifzhudin Noor Aziz: Validation, supervision; Cheng Cheng: Methodology, writing – review & editing; Benchawan Wiwatanapataphee: Writing – review & editing, validation. All authors have read and approved the final version of the manuscript for publication.

Use of Generative-AI tools declaration

All the authors declare that they have not used artificial intelligence (AI) tools in the creation of this article.

Conflict of interest

The authors declare that they have no known competing financial interests or personal relationships that could have appeared to influence the work reported in this paper.

Prof. Benchawan Wiwatanapataphee is the Guest Editor of special issue "Innovative Advances in Mathematical Modeling and Simulation of Complex Systems" for AIMS Mathematics. Prof. Benchawan Wiwatanapataphee was not involved in the editorial review and the decision to publish this article.

References

1. I. Chakraborty, P. Maity, COVID-19 outbreak: Migration, effects on society, global environment and prevention, *Sci. Total Environ.*, **728** (2020), 138882. https://doi.org/10.1016/j.scitotenv.2020.138882

2. N. Shrestha, M. Y. Shad, O. Ulvi, M. H. Khan, A. Karamehic-Muratovic, U. S. D. Nguyen, et al., The impact of COVID-19 on globalization, *One Health*, **11** (2020), 100180. https://doi.org/10.1016/j.onehlt.2020.100180

3. S. Naseer, S. Khalid, S. Parveen, K. Abbass, H. Song, M. V. Achim, COVID-19 outbreak: Impact on global economy, *Front. Public Health*, **10** (2023), 1009393. https://doi.org/10.3389/fpubh.2022.1009393

4. A. U. M. Shah, S. N. A. Safri, R. Thevadas, N. K. Noordin, A. A. Rahman, Z. Sekawi, et al., COVID-19 outbreak in Malaysia: Actions taken by the Malaysian government, *Int. J. Infect. Dis.*, **97** (2020), 108–116. https://doi.org/10.1016/j.ijid.2020.05.093

5. W. O. Kermack, A. G. McKendrick, A contribution to the mathematical theory of epidemics, *Proc. Roy. Soc. Lond. A*, **115** (1927), 700–721. https://doi.org/10.1098/rspa.1927.0118

6. I. Cooper, A. Mondal, C. G. Antonopoulos, A SIR model assumption for the spread of COVID-19 in different communities, *Chaos Soliton. Fract.*, **139** (2020), 110057. https://doi.org/10.1016/j.chaos.2020.110057

7. Y. C. Chen, P. E. Lu, C. S. Chang, T. H. Liu, A time-dependent SIR model for COVID-19 with undetectable infected persons, *IEEE T. Netw. Sci. Eng.*, **7** (2020), 3279–3294. https://doi.org/10.1109/TNSE.2020.3024723

8. S. He, Y. Peng, K. Sun, SEIR modeling of the COVID-19 and its dynamics, *Nonlinear Dyn.*, **101** (2020), 1667–1680. https://doi.org/10.1007/s11071-020-05743-y

9. S. Annas, M. I. Pratama, M. Rifandi, W. Sanusi, S. Side, Stability analysis and numerical simulation of SEIR model for pandemic COVID-19 spread in Indonesia, *Chaos Soliton. Fract.*, **139** (2020), 110072. https://doi.org/10.1016/j.chaos.2020.110072

10. I. Korolev, Identification and estimation of the SEIRD epidemic model for COVID-19, *J. Econometrics*, **220** (2021), 63–85. https://doi.org/10.1016/j.jeconom.2020.07.038

11. S. S. Musa, S. Qureshi, S. Zhao, A. Yusuf, U. T. Mustapha, D. He, Mathematical modeling of COVID-19 epidemic with effect of awareness programs, *Infect. Dis. Model.*, **6** (2021), 448–460. https://doi.org/10.1016/j.idm.2021.01.012

12. Y. Chen, Y. R. Gel, M. V. Marathe, H. V. Poor, A simplicial epidemic model for COVID-19 spread analysis, *Proc. Natl. Acad. Sci.*, **121** (2024), e2313171120. https://doi.org/10.1073/pnas.2313171120

13. C. Cheng, E. Aruchunan, M. H. N. Aziz, Leveraging dynamics informed neural networks for predictive modeling of COVID-19 spread: A hybrid SEIRV-DNNs approach, *Sci. Rep.*, **15** (2025), 2043. https://doi.org/10.1038/s41598-025-85440-1

14. Y. Chen, F. Liu, Q. Yu, T. Li, Review of fractional epidemic models, *Appl. Math. Model.*, **97** (2021), 281–307. https://doi.org/10.1016/j.apm.2021.03.044

15. P. A. Naik, M. Farman, A. Zehra, K. S. Nisar, E. Hincal, Analysis and modeling with fractal-fractional operator for an epidemic model with reference to COVID-19 modeling, *Part. Differ. Equ. Appl. Math.*, **10** (2024), 100663. https://doi.org/10.1016/j.padiff.2024.100663

16. R. Zarin, A. Khan, A. Yusuf, S. Abdel-Khalek, M. Inc, Analysis of fractional COVID-19 epidemic model under Caputo operator, *Math. Method. Appl. Sci.*, **46** (2023), 7944–7964. https://doi.org/10.1002/mma.7294

17. A. Abbes, A. Ouannas, N. Shawagfeh, H. Jahanshahi, The fractional-order discrete COVID-19 pandemic model: Stability and chaos, *Nonlinear Dyn.*, **111** (2023), 965–983. https://doi.org/10.1007/s11071-022-07766-z

18. H. D. S. Adam, M. Althubyani, S. M. Mirgani, S. Saber, An application of Newton's interpolation polynomials to the zoonotic disease transmission between humans and baboons system based on a time-fractal fractional derivative with a power-law kernel, *AIP Adv.*, **15** (2025), 045217. https://doi.org/10.1063/5.0253869

19. M. Althubyani, S. Saber, Hyers-Ulam stability of fractal-fractional computer virus models with the Atangana-Baleanu operator, *Fractal Fract.*, **9** (2025), 158. https://doi.org/10.3390/fractalfract9030158

20. S. Saber, E. Solouma, R. A. Alharb, A. Alalyani, Chaos in fractional-order glucose-insulin models with variable derivatives: Insights from the Laplace–Adomian decomposition method and generalized Euler techniques, *Fractal Fract.*, **9** (2025), 149. https://doi.org/10.3390/fractalfract9030149

21. A. Turab, R. Shafqat, S. Muhammad, M. Shuaib, M. F. Khan, M. Kamal, Predictive modeling of hepatitis B viral dynamics: A Caputo derivative-based approach using artificial neural networks, *Sci. Rep.*, **14** (2024), 21853. https://doi.org/10.1038/s41598-024-70788-7

22. A. Alsulami, R. A. Alharb, T. M. Albogami, N. H. Eljaneid, H. D. Adam, S. F. Saber, Controlled chaos of a fractal-fractional Newton-Leipnik system, *Thermal Sci.*, **28** (2024), 5153–5160. https://doi.org/10.2298/TSCI2406153A

23. M. Alhazmi, F. M. Dawalbait, A. Aljohani, K. O. Taha, H. D. Adam, S. Saber, Numerical approximation method and chaos for a chaotic system in sense of Caputo-Fabrizio operator, *Thermal Sci.*, **28** (2024), 5161–5168. https://doi.org/10.2298/TSCI2406161A

24. A. Turab, H. Hilmi, J. L. G. Guirao, S. Jalil, N. Chorfi, P. O. Mohammed, The Rishi transform method for solving multi-high order fractional differential equations with constant coefficients, *AIMS Math.*, **9** (2024), 3798–3809. https://doi.org/10.3934/math.2024187

25. D. Denu, S. Kermausuor, Analysis of a fractional-order COVID-19 epidemic model with lockdown, *Vaccines*, **10** (2022), 1773. https://doi.org/10.3390/vaccines10111773

26. M. A. A. Oud, A. Ali, H. Alrabaiah, S. Ullah, M. A. Khan, S. Islam, A fractional order mathematical model for COVID-19 dynamics with quarantine, isolation, and environmental viral load, *Adv. Differ. Equ.*, **2021** (2021), 1–19. https://doi.org/10.1186/s13662-021-03265-4

27. S. Paul, A. Mahata, S. Mukherjee, P. C. Mali, B. Roy, Fractional order SEIQRD epidemic model of COVID-19: A case study of Italy, *PLoS One*, **18** (2023), e0278880. https://doi.org/10.1371/journal.pone.0278880

28. E. C. de Oliveira, J. A. T. Machado, A review of definitions for fractional derivatives and integral, *Math. Probl. Eng.*, **2014** (2014), 1–7. https://doi.org/10.1155/2014/238459

29. G. S. Teodoro, J. T. Machado, E. C. de Oliveira, A review of definitions of fractional derivatives and other operators, *J. Comput. Phys.*, **388** (2019), 195–208. https://doi.org/10.1016/j.jcp.2019.03.008

30. R. Agarwal, P. Airan, R. P. Agarwal, Exploring the landscape of fractional-order models in epidemiology: A comparative simulation study, *Axioms*, **13** (2024), 545. https://doi.org/10.3390/axioms13080545

31. S. Rosa, D. F. M. Torres, Numerical fractional optimal control of respiratory syncytial virus infection in Octave/Matlab, *Mathematics*, **11** (2023), 1511. https://doi.org/10.3390/math11061511

32. Y. Bo, C. Guo, C. Lin, Y. Zeng, H. B. Li, Y. Zhang, et al., Effectiveness of non-pharmaceutical interventions on COVID-19 transmission in 190 countries from 23 January to 13 April 2020, *Int. J. Infect. Dis.*, **102** (2021), 247–253. https://doi.org/10.1016/j.ijid.2020.10.066

33. A. Mendez-Brito, C. El Bcheraoui, F. Pozo-Martin, Systematic review of empirical studies comparing the effectiveness of non-pharmaceutical interventions against COVID-19, *J. Infect.*, **83** (2021), 281–293. https://doi.org/10.1016/j.jinf.2021.06.018

34. A. Lison, N. Banholzer, M. Sharma, S. Mindermann, H. J. T. Unwin, S. Mishra, et al., Effectiveness assessment of non-pharmaceutical interventions: Lessons learned from the COVID-19 pandemic, *Lancet Public Health*, **8** (2023), e311–e317. https://doi.org/10.1016/S2468-2667(23)00046-4

35. B. A. Baba, B. Bilgehan, Optimal control of a fractional order model for the COVID-19 pandemic, *Chaos Soliton. Fract.*, **144** (2021), 110678. https://doi.org/10.1016/j.chaos.2021.110678

36. T. Trisilowati, I. Darti, R. R. Musafir, M. Rayungsari, A. Suryanto, Dynamics of a fractional-order COVID-19 epidemic model with quarantine and standard incidence rate, *Axioms*, **12** (2023), 591. https://doi.org/10.3390/axioms12060591

37. K. Diethelm, Monotonicity of functions and sign changes of their Caputo derivatives, *Fract. Calc. Appl. Anal.*, **19** (2016), 561–566. https://doi.org/10.1515/fca-2016-0029

38. S. Majee, S. Jana, D. K. Das, T. K. Kar, Global dynamics of a fractional-order HFMD model incorporating optimal treatment and stochastic stability, *Chaos Soliton. Fract.*, **161** (2022), 112291. https://doi.org/10.1016/j.chaos.2022.112291

39. J. Danane, Z. Hammouch, K. Allali, S. Rashid, J. Singh, A fractional-order model of coronavirus disease 2019 (COVID-19) with governmental action and individual reaction, *Math. Method. Appl. Sci.*, **46** (2023), 8275–8288. https://doi.org/10.1002/mma.7759

40. D. D. Hailemichael, K. E. Geremew, P. R. Koya, Effect of vaccination and culling on the dynamics of rabies transmission from stray dogs to domestic dogs, *Hind J. Appl. Math.*, **2022** (2022), 2769494. https://doi.org/10.1155/2022/2769494

41. O. Diekmann, J. A. P. Heesterbeek, *Mathematical epidemiology of infectious diseases: Model building, analysis and integration*, New York: Wiley, 2000.

42. E. Ahmed, A. M. A. El-Sayed, H. A. El-Saka, On some Routh–Hurwitz conditions for fractional order differential equations and their applications in Lorenz, Rössler, Chua and Chen systems, *Phys. Lett. A*, **358** (2006), 1–4. https://doi.org/10.1016/j.physleta.2006.04.087

43. G. Z. Lin, L. L. Hao, Stability of a SEIQR epidemic model with infectious incubation period and infectious period, *J. Southwest China Normal Univ. (Nat. Sci. Ed.)*, **45** (2020), 1–4. https://doi.org/10.13718/j.cnki.xsxb.2020.03.001

44. J. P. La Salle, *The stability of dynamical systems*, Philadelphia: Society for Industrial and Applied Mathematics, 1976. https://doi.org/10.1137/1.9781611970432

45. N. Águila-Camacho, M. A. Duarte-Mermoud, J. A. Gallegos, Lyapunov functions for fractional order systems, *Commun. Nonlinear Sci. Numer. Simul.*, **19** (2014), 2951–2957. https://doi.org/10.1016/j.cnsns.2014.01.022

46. C. Vargas-De-León, Volterra-type Lyapunov functions for fractional-order epidemic systems, *Commun. Nonlinear Sci. Numer. Simul.*, **24** (2015), 75–85. https://doi.org/10.1016/j.cnsns.2014.12.013

47. J. Li, X. Tan, W. Wu, X. Zou, A Caputo fractional derivative dynamic model of hepatitis E with optimal control based on particle swarm optimization, *AIP Adv.*, **14** (2024), 045125. https://doi.org/10.1063/5.0193463

48. I. M. Elbaz, M. A. Sohaly, H. El-Metwally, Random dynamics of an SIV epidemic model, *Commun. Nonlinear Sci. Numer. Simul.*, **131** (2024), 107779. https://doi.org/10.1016/j.cnsns.2023.107779

49. R. Garrappa, Numerical solution of fractional differential equations: A survey and a software tutorial, *Mathematics*, **6** (2018), 16. https://doi.org/10.3390/math6020016

50. R. Garrappa, On linear stability of predictor-corrector algorithms for fractional differential equations, *Int. J. Comput. Math.*, **87** (2010), 2281–2290. https://doi.org/10.1080/00207160802624331

51. *Ministry of Health Malaysia, COVID-19 public data*, 2024. Available from: `https://github.com/MoH-Malaysia/covid19-public`.

52. N. Sene, Analysis of the fractional SEIR epidemic model with Caputo derivative via resolvent operators and numerical scheme, *Discrete Cont. Dyn.-S*, **18** (2025), 1316–1330. https://doi.org/10.3934/dcdss.2024149

53. L. S. Pontryagin, *Mathematical theory of optimal processes*, Routledge, 2018. http://dx.doi.org/10.1201/9780203749319

54. S. I. Oke, M. B. Matadi, S. S. Xulu, Cost-effectiveness analysis of optimal control strategies for breast cancer treatment with ketogenic diet, *Far East J. Appl. Math.*, **109** (2018), 303–342. http://dx.doi.org/10.17654/MS109020303

55. *Ministry of Health Malaysia, MOH Spends RM18,000 Per Critically Sick COVID-19 Patient*, CodeBlue, 2020. Available from: `https://codeblue.galencentre.org/2020/07/moh-spends-rm18000-per-critically-sick-covid-19-patient/`.

AIMS Press

© 2025 the Author(s), licensee AIMS Press. This is an open access article distributed under the terms of the Creative Commons Attribution License (https://creativecommons.org/licenses/by/4.0)